Coronary blood vessels from distinct origins converge to equivalent states during mouse and human development

Ragini Phansalkar[1,2], Josephine Krieger[2], Mingming Zhao[4,5], Sai Saroja Kolluru[6,7], Robert C. Jones[6], Stephen R Quake[6,7], Irving Weissman[3], Daniel Bernstein[4,5], Virginia D. Winn[8], Gaetano D'Amato[2]*, Kristy Red-Horse[2,3,5]*

1. Department of Genetics, Stanford University School of Medicine, Stanford, CA, 94305, USA
2. Department of Biology, Stanford University, Stanford, CA, 94305, USA
3. Institute for Stem Cell Biology and Regenerative Medicine, Stanford University School of Medicine, Stanford, CA, 94305, USA
4. Division of Pediatric Cardiology, Department of Pediatrics, Stanford University School of Medicine, Stanford, CA, 94305, UCA
5. Stanford Cardiovascular Institute, Stanford University School of Medicine, Stanford, CA, 94305, USA
6. Department of Bioengineering and Department of Applied Physics, Stanford University, Stanford, CA, 94305, USA
7. Chan Zuckerberg Biohub, Stanford, CA, 94305, USA
8. Department of Obstetrics and Gynecology, Stanford University School of Medicine, Stanford, CA, 94305, USA

*Corresponding Authors: kredhors@stanford.edu, damatog@stanford.edu

Abstract

Most cell fate trajectories during development follow a diverging, tree-like branching pattern, but the opposite can occur when distinct progenitors contribute to the same cell type. During this convergent differentiation, it is unknown if cells “remember” their origins transcriptionally or whether this influences cell behavior. Most coronary blood vessels of the heart develop from two different progenitor sources—the endocardium (Endo) and sinus venosus (SV)—but whether transcriptional or functional differences related to origin are retained is unknown. We addressed this by combining lineage tracing with single-cell RNA sequencing (scRNAseq) in embryonic and adult mouse hearts. Shortly after coronary development begins, capillary ECs transcriptionally segregated into two states that retained progenitor-specific gene expression. Later in development, when the coronary vasculature is well-established but still remodeling, capillary ECs again segregated into two populations, but transcriptional differences were related to tissue localization rather than lineage. Specifically, ECs in the heart septum expressed genes indicative of increased local hypoxia and decreased blood flow. Adult capillary ECs were more homogeneous and lacked indications of either lineage or location. In agreement, SV- and Endo-derived ECs in adult hearts displayed similar responses to injury. Finally, scRNAseq of developing human coronary vessels indicated that the human heart followed similar principles. Thus, over the course of development, transcriptional heterogeneity in coronary ECs is first influenced by lineage, then by location, until heterogeneity disappears in the homeostatic adult heart. These results highlight the plasticity of ECs during development, and the validity of the mouse as a model for human coronary development.

Introduction

During embryonic development, progenitor tissue sources produce new cell types through shifts in epigenetic and transcriptional states. Much research addresses how new cell types form, yet there is less focus on how the transcriptional or chromatin states of progenitors cells relate to gene expression in their descendants, i.e. what do mature cells “remember” about their history? This question is particularly intriguing in cases where multiple progenitor sources contribute to the same cell type, since different origins could result in different behaviors or responses to injury and disease. Such lineage merging is referred to as “convergent differentiation” and occurs in hematopoietic populations (Sathe et al., 2013; Weinreb et al., 2020), oligodendrocytes (Marques et al., 2018), olfactory projection neurons (Li et al., 2017), coronary blood vessels of the heart (Sharma et al., 2017), and others (Wei et al., 2015; Gerber et al., 2018; Konstantinides et al., 2018). Recent single-cell RNA sequencing (scRNAseq) analyses have suggested that the resulting cell types can converge transcriptionally (Li et al., 2017), but in some cases maintain molecular signatures of their progenitors (Dick et al., 2019; Weinreb et al., 2020). However, there is no information on how convergent differentiation influences coronary blood vessels of the heart or how this might affect cardiac injury responses.

In this study, we investigated gene expression patterns in two lineage trajectories that form the coronary vasculature in mice and compared these with data from human fetal hearts. The major progenitor sources for coronary endothelial cells (ECs) in mice are the sinus venosus (SV), the venous inflow tract of the developing heart, and the endocardium (Endo), the inner lining of the heart ventricles (Red-Horse et al., 2010; Wu et al., 2012; Chen et al., 2014; Tian et al., 2014; Zhang et al., 2016; Sharma et al., 2017; Su et al., 2018). ECs begin to migrate from both these sources at embryonic day 11.5. They form an immature capillary plexus (Zeini et al., 2009; Red-Horse et al., 2010) by populating the heart with vessels from the outside-in (SV) or the inside-out

(Endo). These two sources eventually localize to largely complimentary regions: the SV contributes vessels to the outer myocardial wall and the Endo contributes vessels to the inner myocardial wall and the septum (Red-Horse et al., 2010; Wu et al., 2012; Chen et al., 2014; He et al., 2014; Tian et al., 2014; Zhang et al., 2016; Sharma et al., 2017). Initial angiogenesis from the SV or Endo is guided by different signaling factors (Wu et al., 2012; Arita et al., 2014; Chen et al., 2014; Su et al., 2018; Payne et al., 2019). However, in circumstances where SV angiogenesis is stunted, Endo-derived vasculature can expand into the outer wall to compensate for the vessel loss (Sharma et al., 2017).

In contrast to the well-characterized spatial differences between Endo and SV angiogenesis, there have been no comparisons of transcriptional states between Endo- and SV-derived coronary vessels, in development or in adulthood. In addition, there is little information on whether coronary ECs in humans are also derived from these sources, or whether the transcriptional/functional states that human coronary ECs pass through during development match those in the mouse. Understanding any lineage-specific or species-specific traits would have important implications for approaches that reactivate developmental pathways to increase angiogenesis in injured or diseased human hearts (Smart, 2017; Payne et al., 2019).

Here, we used scRNAseq of lineage-traced ECs from mouse hearts at various stages of development to show that while SV- and Endo-derived capillary cells initially retained some source-specific gene expression patterns, these differences were only present at an early stage of development. Later, these lineages mixed into two capillary subtypes, which were correlated with different locations in the heart. By adult stages, SV- and Endo-derived cells had converged into a largely homogenous population of capillary ECs, and differing lineage did not result in differential proliferation in response to ischemia/reperfusion (IR)-induced injury. Finally, scRNAseq on human fetal hearts indicated that human development closely matched that in mice,

and provided additional insights into human coronary artery development. Based on our results, we propose a model in which the transcriptional state of coronary ECs is initially influenced by their lineage, then by regional differences in environmental factors, and finally settles on a single state by adulthood when these regional differences fade. These findings highlight the importance of environmental factors in influencing EC behavior, and validate mice as a representative model for human coronary development.

Results

ScRNAseq in lineage-labeled coronary ECs

To compare Endo- and SV-derived ECs during development and in adult hearts, we combined scRNAseq with lineage-specific fluorescent labeling (Fig. 1a and b). For embryonic hearts, a Tamoxifen-inducible *BmxCreER* (Ehling et al., 2013) mouse was crossed with the *Rosa*^{tdTomato} Cre reporter, which specifically labels a high percentage of the Endo (94.44% of Endo cells labeled at e12.5), but does not mark the SV (3.61% of SV cells labeled at e12.5)(D'Amato et al., *in preparation*). Labeling was induced before e11.5, when coronary development begins, so Endo-derived ECs expressed *tdTomato* while SV-derived ECs did not. Cells from e12 and e17.5 hearts were FACS sorted and processed using the 10X Genomics platform (Fig. 1a and S1). For adult hearts, we used either *BmxCreER* to label the Endo or *ApjCreER* (Chen et al., 2014) to label the SV during development. FACS sorting was used to isolate lineage specific ECs, but scRNAseq was performed using Smart-seq2 (Picelli et al., 2014)(Fig. 1b). This more sensitive platform was employed since quiescent adult cells are known to have less mRNA content and preliminary studies indicated less heterogeneity in coronary ECs at this time (Anisimova et al., 2020; Gulati et al., 2020). These strategies captured the expected EC subtypes at each stage (including coronary, valve, Endo, SV, lymphatics)(Fig. S2a and b) and contained a large number of cells that passed standard quality controls (Methods). ScRNAseq analyses are most accurate when

the cell populations being compared are extracted and re-analyzed without the influence of data from unrelated or cycling cell types in the dataset (Luecken and Theis, 2019). Thus, we isolated non-cycling coronary ECs (for e12— *Pecam1+, Cldn5+, Npr3-, Top2a-, Mki67-, Tbx20-, Cldn11-, Bmp4-, Vwf-*; for e17.5—*Pecam1+, Npr3-, Tbx20-, Pdgfra-, Top2a-, Bmp4-, Mki67-*)(Fig. S2c and d) and performed direct comparisons of cell states between Endo- and SV-derived coronary ECs. The remaining cells in the dataset will be reported by D'Amato et al., which addressed experimental questions outside the scope of this study.

We first used unbiased clustering to identify coronary EC subtypes within the e12, e17.5, and adult datasets. E12 coronary ECs separated into three clusters—capillary plexus 1 (Cap1), capillary plexus 2 (Cap2), and pre-artery (Fig. 1c). Markers used to identify these populations matched previous reports and are shown in Fig. S3a. The absence of venous ECs and the higher numbers of SV-enriched cells present at this stage are also consistent with previous studies (Red-Horse et al., 2010; Su et al., 2018). Separating plots by sample revealed that Cap2 was exclusively from the SV-enriched sample (Fig. 1d and e). Consistent with this was its increased expression of *Apj* (*Aplnr*)(Fig. S3a), which we previously demonstrated to be enriched in SV-derived vessels (Sharma et al., 2017). Cap1 had a higher number of cells from the Endo, but also contained cells from the SV-enriched sample (Fig. 1d and e). Although recombination rates in the Endo were very high (Methods), we cannot exclude the possibility that a small number of Endo-derived ECs are *tdTomato*-negative due to some un-recombined Endo ECs. These data show that shortly after coronary development is initiated, lineage is correlated with transcriptionally distinct capillary populations within the immature capillary plexus.

To test whether this phenomenon persists into late development, we similarly analyzed coronary ECs at e17.5. A larger number of coronary ECs were captured due to the increase in cardiac vasculature by this stage. EC clusters in this sample included two artery (Art1 and Art2), one vein,

and two capillary (Cap1 and Cap2) clusters (Fig. 1f and S3b). If Cap1 and Cap2 continued to reflect different lineages, we would expect at least one cluster to contain only Endo- or SV-enriched ECs. There was skewed contribution with a higher percentage of Endo-enriched cells in Cap1 and a higher percentage of SV-enriched cells in Cap2 (Fig. 1g and h), but no cluster was lineage exclusive, suggesting that other factors were driving transcriptional heterogeneity. Veins were much more represented in the SV-enriched sample (Fig. 1h), which is expected since most veins reside on the surface of the heart and SV angiogenesis progresses outside-in while Endo angiogenesis is in the opposite direction. Additionally, when cycling cells were included in the analysis, a similar pattern of lineage contribution was observed, and Cap1 and Cap2 each contained a similar percentage of cycling cells (Fig. S4d and e).

We next performed the same analyses on adult coronary ECs. Fewer cells were captured since Smart-seq2 was the method of choice at this stage to obtain maximum read depth (Fig. 1b). Clustering revealed one artery, one vein, and two capillary clusters (Cap1 and Cap2)(Fig. 1i and S3c). Similar to e17.5, Cap1 and Cap2 showed a slightly skewed, but not exclusive, representation among the lineages (Fig. 1j-k). However, unlike the clusters at earlier stages that were distinguished by >150 genes, adult Cap1 and Cap2 had only 11 differentially expressed genes passing the same log fold change and p-value cutoffs. This indicated that these two clusters are likely transcriptionally and functionally more similar than the two clusters at e12 and e17.5. Their increased similarity can also be observed in the UMAP reduction of the adult data where they largely overlap (Fig. 1i), which is in contrast to the spatial segregation of Cap1 and Cap2 in the e12 and e17.5 UMAPs (Fig. 1c and f). We considered whether the adult capillary homogeneity was influenced by the smaller number of cells typical for Smart-seq2. A publicly available adult heart EC dataset generated by Kalucka et al. (Kalucka et al., 2020) using 10X Genomics contained one additional small cluster (Fig. S5a). This cluster was marked by *Apln*, and we found an analogous subset of *Apln*+ cells in our data despite them not separating into their own cluster.

The *Apln*+ cells were equally represented by Endo- and SV-derived cells, indicating that this additional subset of cells is not lineage specific (Fig. S5c). This was supported by a prior study in which *Apln*+ cells in adult hearts were not observed to be specifically localized to either the septum or the inner or outer myocardial wall (Liu et al., 2015). Therefore, we concluded that there is no lineage-based heterogeneity in adult coronary ECs.

Coronary heterogeneity is first related to lineage and then to location

We next investigated the genes driving coronary ECs into two capillary cell states at the different stages of development. One hypothesis was that they retained gene expression patterns from their progenitors. To test this, a list of genes defining the Endo and SV at e12 was compiled, and their expression assessed in capillary clusters. At e12, Cap1 cells expressed higher levels of Endo-specific genes, while Cap2 cells expressed higher levels of SV-specific genes (Fig. 2a and S6 a-c). Indeed, 40% of Cap1 genes and 3% of Cap2 genes overlapped with the Endo, while 47% of Cap2 genes and 1% of Cap1 genes overlapped with the SV (Fig. 2b). We concluded that the transcriptional identities of Cap1 and Cap2 cells derive at least in part by gene expression patterns retained from the SV or Endo.

This same pattern was not observed at e17.5. There were no clear pattern between e17.5 Cap1 and Cap2 in the expression of SV- and Endo-specific genes (Fig. 2a and S6d), and there was little to no overlap between Cap1 and Cap2 differential genes and SV or Endo genes (Fig. 2c). Furthermore, there was minimal overlap between the e12 and e17.5 Cap1 and Cap2 defining genes, which is consistent with e17.5 coronary ECs not retaining the progenitor-type genes enriched in e12 clusters (Fig. 2d). Calculating Pearson correlations using Endo and SV genes also revealed that e12 coronary ECs were similar to their progenitor sources while e17.5 coronary ECs were much less so (Fig. 2e). We also calculated Pearson correlations as a function of lineage

at e12. As expected, *tdTomato* positive cells were highly similar to the Endo while *tdTomato* negative cells in Cap2 were similar to the SV than to the Endo (Fig. 2f). Interestingly, *tdTomato* negative cells in Cap1 were more similar to the Endo than to the SV (Fig. 2f). This could result from a number of reasons that we cannot currently distinguish including: 1) SV-derived cells migrating close to the Endo take on Endo-type gene expression or 2) There is a rare Endo population that does not express *Bmx*. The latter is supported over the former due to the observation that Cap2-like cells are present in a previous scRNAseq dataset of SV-derived ECs (Su et al., 2018), while Cap1 cells are not (Fig. S7d and e). Finally, we confirmed that adult capillary clusters do not retain Endo and SV gene expression, which is expected given the very few differentially expressed genes (DEGs) detected between adult Cap1 and Cap2 (Fig. 2g). In total, these data indicate that e17.5 capillary heterogeneity was neither caused by lineage nor a remnant of the heterogeneity present at e12, and lineage-related differences were not apparent in adults.

We next considered whether differential localization in the heart might underlie e17.5 heterogeneity. During development, different regions of the heart show varying levels of hypoxia and signaling factors, e.g. at some stages, the septum is more hypoxic and expresses higher levels of *Vegfa* (Miquerol et al., 2000; Sharma et al., 2017). Localization-driven heterogeneity would also explain the bias in cluster distribution between the Endo and SV lineages (Fig. 1h) because they contribute ECs to complementary regions of the heart. This is most dramatic in the septum where almost all ECs are derived from the Endo (Wu et al., 2012; Chen et al., 2014; Zhang et al., 2016). The top DEGs between e17.5 Cap1 and Cap2 included hypoxia-induced genes (*Mif, Adm, Igfbp3, Kcne3*)(Tazuke et al., 1998; Lee et al., 1999; Keleg et al., 2007; Simons et al., 2011; Heng et al., 2019) and tip cell markers (*Apln, Plaur, Lamb1, Dll4*)(Hellstrom et al., 2007; del Toro et al., 2010) in Cap1, and flow-induced genes (*Klf2, Klf4, Thbd, Lims*) (Dekker et

al., 2002; Hamik et al., 2007; Kumar et al., 2014; Wang and Zhang, 2020) in Cap2 (Fig. 3a and b, Fig. S8), suggesting pathways that could be consistent with localization-driven heterogeneity.

We next used Car4 to localize Cap2 within the tissue because it was differentially expressed in this cluster and there was an antibody available for immunostaining (Fig. 3a and c). Erg-positive ECs expressing Car4 were located mainly in the right and left ventricle free walls and dorsal side while those in the septum and ventral wall were mostly negative (Fig. 3d and e). This indicated that Cap1 localizes primarily to the septum and ventral wall and Cap2 to the remaining walls of the ventricle. The *Kcne3* pattern provided further support for this localization because it was specific to Cap1, and *in situ* hybridization revealed strong septal and ventral expression (Fig. 3f). Car4 analysis revealed a further segregation of Cap1 into septum and non-septum regions on the UMAP. Specifically, one side of the Cap1 cluster was almost completely devoid of Car4 and comprised almost all Endo-derived cells (Fig. 3c), which are two features specific to the septum as shown in Fig. 3d and e. Interestingly, this septum region is where gene expression indicates both decreased blood flow and local hypoxia (Fig. 3b), the former of which would cause the latter. Thus, the coronary vasculature in the septum (and where the rest of Cap1 localizes) may not receive full blood flow at this late stage in development.

With the knowledge that half of Cap1 was almost completely represented by Endo-derived cells from the septum, we manually searched for whether any Endo-specific genes expression was retained only in those cells. A few of the Endo-specific genes were specifically expressed in this regions while a few SV-specific genes were excluded (Fig. S9), indicating that there could be some retention of transcriptional patterns from progenitors states. However, this may be a minor observation because only 10 Endo genes and 6 SV genes fit this pattern, most of which were expressed by less than 20% of the capillary cells (Fig. S9).

To probe whether the septal portion of Cap1 (see Fig. 3c, dotted line) segregates based on cell-autonomous, lineage-specific features of Endo-derived ECs or regional environments, we took advantage of the fact that some Endo-lineage labeled cells migrate into SV-biased territories during development (Chen et al., 2014). Cell-autonomous lineage differences would be supported if these cells remained Car4-negative in the ventricular walls. However, the opposite was true. Endo-lineage cells in ventricular walls were more likely to express Car4 than those in the septum (on average, 23% outside septum vs. 4% inside septum)(Fig. 3e). Endo-derived ECs in SV-biased territories such as the dorsal side of the heart start to express Car4 (Fig. 3d, arrows), and they can exist in the Cap2 state (Fig. 3c, arrow). Thus, the combination of lineage labeling, scRNAseq, and histology allowed us to ascertain that Endo-lineage ECs are biased towards a separate cell state based on their preferential location in hypoxic regions; however, if they migrate into SV-biased territories during angiogenesis, they are capable of becoming transcriptionally similar to SV-derived cells.

Since regional hypoxia would be incompatible with adult heart function, we predicted that the absence of strong heterogeneity in adult capillary ECs could be explained by a resolution of regional environmental differences after development. To test this, we focused on the septum, which was physically separated during adult processing (see Fig. 1b and Methods) to produce a “septum-enriched” sample. We found that the cells from this sample were evenly distributed between adult Cap1 and Cap2, intermingled with the other capillaries on the UMAP, and were now positive for *Car4* (Fig. 3g). Immunostaining confirmed that septum ECs had become positive for Car4 in adults (Fig. 3h). Altogether, our data support the following model—that over the course of development, transcriptional heterogeneity in coronary ECs is first influenced by lineage, then by location, until both lineage- and location-based heterogeneity disappears in the static adult heart (Fig. 3i).

Lineage does not change response to ischemia-reperfusion injury

Although Endo- and SV-derived capillary ECs were transcriptionally very similar in normal adult hearts, they could behave differently when challenged with hypoxia or other injury. To test this, we performed an ischemia-reperfusion (IR) injury by temporarily occluding the left anterior descending (LAD) coronary artery in adult *BmxCreER;Rosa*^{tdTomato} mouse hearts in which the Endo was labelled prior to coronary development (Fig. 4a and S1b). Proliferation in Endo- and SV-enriched ECs was quantified using EdU incorporation assays on day 5 post-injury. This time point was chosen based on prior data showing regrowth of the majority of coronary vessels 5 days after IR injury (Merz et al., 2019). Observing overall EdU incorporation revealed the site of injury, which was prominent in the mid-myocardial region between the inner and outer wall (Fig. 4b). Proliferation was assessed in areas just below the ligation and apex of the heart, as this is the expected distribution of ischemia following LAD ligation (Merz et al., 2019). Regions of interest were chosen in myocardial areas containing a mix of Endo- and SV-derived ECs to ensure adequate representation from both lineages (Fig. 4c and d). This analysis found no difference between the lineages (Fig. 4e). We next performed EdU quantification in the inner and outer walls of the myocardium where most ECs derive from either the Endo or SV, respectively (Wu et al., 2012; Tian et al., 2014; Zhang et al., 2016; Sharma et al., 2017)(Fig. 4b and S1b and c). In contrast to the lineage comparison, the outer wall showed a consistent, though non-significant, increase in EC proliferation over the inner wall, both within and adjacent to the injury site and regardless of lineage, indicating that this injury and proliferation assay can reveal differences (Fig. 4f). These data support the notion that location, and not lineage, regulates capillary responses to injury in adult hearts, at least with respect to EC proliferation in the days after injury.

Analogous features in mouse and human coronary ECs

We next sought to investigate whether comparing mouse and human scRNAseq datasets could provide insights into human development. ScRNAseq was performed using Smart-seq2 on CD31-positive ECs sorted from human fetal hearts at 11, 14, and 22 weeks of gestation. In addition, a capillary-specific marker, CD36, allowed for enrichment of CD31+CD36- arterial ECs (Fig. 5a and S10a and b) (Cui et al., 2019). After initial filtering, 2339 high-quality, high-coverage single EC transcriptomes were obtained of which 713 were arterial. The data included 12 clusters of the expected cells types—artery, capillary, vein, cycling, Endo, valve EC—identified by known markers (Fig. 5b and S10c). As with the mouse data, the analysis was restricted to non-cycling arteries, capillaries, and veins in order to specifically compare cell states and trajectories in coronary vessels. Similar to mouse, the data contained one vein and two capillary clusters, but contrasting to mouse, there was an additional arterial cluster for a total of three (Fig. 5c). There was approximately equal representation of the clusters in the CD31-positive fraction at each gestational age, consistent with the data being from later stages (mouse equivalent of e15.5-18.5)(Krishnan et al., 2014) when the developing heart is growing in size rather than producing new coronary cell subtypes (Fig. 5d and S11a). Consequently, we pooled data from the three timepoints for all further analyses.

To begin comparing human and mouse, the *Seurat* Label Transfer workflow (Stuart et al., 2019) was utilized to reference map each human cell to its closest mouse cluster and vice versa (Fig. 5e). This showed close concordance between the two species (Fig. 5f and g). With respect to the two capillary clusters that were extensively studied above, the majority of human Cap1 cells mapped to mouse Cap1, while the majority of human Cap2 cells mapped to mouse Cap2 (Fig. 5f). When assigning mouse cells to human clusters, mouse Cap2 almost completely mapped to human Cap2, while mouse Cap1 mapped substantially to human Cap1, Cap2, and Art3 (Fig 5g). Analyzing specific gene expression revealed several enriched genes shared between

corresponding mouse and human capillaries (including *KIT*, *ODC1*, *CD300LG*, *RAMP3*), and showed that human Cap1, like its mouse correlate, displayed patterns indicative of experiencing low blood flow conditions and potentially increased hypoxia, i.e. lower *LIMS2, THBD, KLF2, KLF4* and higher *ADM, IGFBP3, KCNE3, LAMB1* (Fig. 5h and S10d). Notably, *CA4* (the human homolog of mouse *Car4*) was not differentially expressed between human Cap1 and Cap2. Since lineage data and *in situ* immunofluorescence confirmed a subset of mouse Cap1 as containing the Endo-derived cells present in the septum (see Fig. 3c), the human expression data in Fig. 5h suggested that human Cap1 may also represent an enrichment of septal cells with less blood flow and could also be biased towards the Endo lineage, although the latter cannot be confirmed with gene expression alone. When using the Label Transfer workflow to specifically map the putative mouse septal ECs to the human data, a higher percentage of human Cap1 than Cap2 cells matched to this septal EC group (35% of Cap1 cells versus 14% of Cap2 cells) (Fig. S10e). We concluded that similar developmental environments and endothelial cell states exist between mouse and human capillaries, including those unique to the septum (Fig. 5i).

Characterization of the capillary-to-artery transition in human coronary ECs

Because unbiased clustering produced three artery clusters in human but only two in mouse, we next investigated whether human hearts contained an artery cell state not present in mouse. This could occur because mouse and human arteries have some structural differences, e.g. large conducting arteries in humans are on the surface rather than within the myocardium as in mouse (Wessels and Sedmera, 2003; Kumar et al., 2005; Fernandez et al., 2008; Sorop et al., 2020). If these differences translated into an artery transcriptional state unique to human, we would expect one of the human artery clusters to not be represented in the mouse mapping. Instead, mouse cells mapped to all three human artery clusters (Fig. 6a).

There was also evidence indicating that human Art3 cells were in a less mature arterial state compared to human Art1 and 2. This is because: 1) Art3 was unique among the human artery clusters in that a high proportion of Art3 cells matched mouse capillaries (Fig. 6a). 2) Trajectory analysis with RNA velocity (La Manno et al., 2018), Slingshot (Street et al., 2018), and partition-based graph abstraction (PAGA) (Wolf et al., 2019) indicated a transition from human Art3 -> Art2 -> Art1 (Fig. 6b and S11b). and 3) Comparing the fetal dataset with a publicly available adult dataset (Litvinukova et al., 2020) showed that almost no adult human artery ECs mapped to Art3, which would be predicted if Art3 were an immature developmental state (Fig. 6c and S10f). Together, these data suggest that human hearts do not contain a dramatically unique artery transcriptional state when compared to mouse, but they do have an immature state (Art3) that matures into Art1 and Art2 in adults.

Reference mapping from the fetal to adult human datasets also revealed a notable reduction in Cap1 cells (28% of fetal capillary cells are Cap1 versus 6% of adult capillary cells)(Fig. 6c). In mice, e17.5 Cap1 and Cap2 converged into a relatively homogenous capillary population in adult (Fig 1i). The small percentage of adult human coronary ECs mapping to the fetal Cap1 cluster, as well as the spatial overlap between cells mapping to Cap1 and Cap2 in the adult UMAP reduction, indicates that these developmental states related to flow and oxygenation also converge in humans.

We next performed trajectory analysis to investigate whether arteries develop through the differentiation of capillary ECs, which is the developmental pathway in mice (Red-Horse et al., 2010; Su et al., 2018). Two common methods for estimating trajectories, PAGA and Slingshot, identified connections between human Cap1 and Art3 and Cap2 and Art2 (Fig. 6b and S11b). RNA velocity suggested directionality going from the capillaries into arteries (Fig. 6b). These two predicted capillary to artery transitions suggested that Cap1/Art3 and Cap2/Art2 may be

differentiation trajectories occurring in two different locations in the heart, i.e. septum vs. ventricle walls. This is supported by the observation that several genes are specifically co-expressed in Cap1 and Art3 (including *CXCR7*, *MCAM*, and *TNFAIP8L1*, *PGF)* or in Cap2 and Art2 (including *TINAGL1*, *SLC9A3R2*, *SGK1*, *THBD*, *LIMS2*, *CALCRL),* some of which were shared with mouse (Fig. 5h, 6d, and S10g). From these data, we propose a model where, in both mouse and human, two distinct subtypes of capillary cells at different locations in the developing heart initially produce two subtypes of artery cells, one of which eventually matures into the other (Fig. 5i).

Characterization of human artery EC subpopulations

Since coronary artery disease is a leading cause of death and developmental information could suggest regenerative pathways, we next focused on the gene pathways present in developing human coronary arteries. As described above, unbiased clustering resulted in three artery states, each expressing known artery markers such as *GJA4* and *HEY1*, but also containing unique genes (Fig. 7a). The *SCENIC* package (Aibar et al., 2017), which uses gene expression information to identify transcription factor “regulons” present in cells, implicated *SOX17* as being strongly enriched in developing artery ECs (Fig. 7b), which is consistent with previous reports on artery development (Corada et al., 2013; Gonzalez-Hernandez et al., 2020). Transcription factors of potential importance that have not been previously implicated in artery development were *PRDM16* and *GATA2* (Fig. 7b). Interestingly, the *IRF6* regulon was specific to the most mature population suggesting a potential role in artery maturation (Fig. 7c). All of these regulons were similarly enriched in mouse artery cells (Fig. 7b and c). We also identified several genes with strong expression patterns in human artery ECs that were not found in mouse (Fig. 7d and Table 1). Interestingly, these included a GABA receptor, *GABBR2*, which was enriched in Art2, and a Glutamate receptor, *GRIA2*, which was is enriched in Art1. The human cells expressing *GABBR2* also co-expressed *SLC6A6*, a transporter that imports the GABBR2 ligand into cells (Tomi et al.,

2008)(Fig. 7d). Finally, we localized different types of arteries in sections of human fetal hearts. In order to identify the artery subtypes, we used in-situ hybridization for *GJA4* and *GJA5*. We found that *GJA5*-positive ECs, marking Art1, are in a small number of large arteries always covered with smooth muscle, while *GJA5*-negative/*GJA4*-positive ECs, marking Art2 and Art3, are numerous and in some cases not covered with smooth muscle (Fig. 7e and f). This supports the conclusion that Art1 represents artery ECs in larger, more proximal branches, and Art2 and Art3 are smaller arterioles (Fig. 7g).

Discussion

Coronary ECs differentiate predominantly from the Endo and the SV. Although the spatial arrangement of these two lineages in the developing and adult mouse heart have been well characterized, it was previously unknown if either the distinct origin or localization of Endo- and SV-derived cells results in transcriptional or functional differences. Here, we used scRNAseq of lineage-traced ECs to address this question. At e12, when coronary vessels are just beginning to form, ECs transcriptionally segregated into two groups which are correlated with either Endo- or SV-specific expression patterns, and one of which is composed of only SV-lineage cells. However, at e17.5, during a phase of rapid growth and vascular remodeling, ECs segregated primarily based on being localized to either the septum or ventricular walls, the former of which expressed a genetic signature of experiencing low oxygen and blood flow. In adult hearts, Endo- and SV-derived ECs cannot be distinguished either by gene expression or by their level of proliferation in response to IR injury. Altogether, these findings demonstrate that over the course of embryonic and post-natal development, coronary ECs from separate lineages converge both transcriptionally and functionally.

This result is relevant to future studies aiming to use developmental pathways to enhance regeneration in adult hearts. For example, it implies that approaches to stimulate re-growth of the vasculature after myocardial injury will affect all cells equally with regard to lineage, and that achieving vascular remodeling in adults may require replicating specific environmental cues and signals (especially those related to hypoxia and flow). The transcriptional similarity of adult Endo- and SV-derived cells helps explain the prior observation that mutant embryos whose coronary vasculature was derived primarily from the Endo due to compensation for loss of SV sprouting grew into phenotypically normal adults despite developmental defects (Sharma et al., 2017). It also raises additional questions for investigation, namely, how is it that coronary ECs can over time lose the signatures both of their progenitors (between e12 and e17.5) and of their developmental "home" (between e17.5 and adult)? The unexpected plasticity of these embryonic cells in their ability to become completely transcriptionally identical represents a potential model for efforts to stimulate faithful differentiation of very specific cell types from induced pluripotent stem cells or non-canonical progenitors (Yamanaka, 2020).

Another outstanding question addressed by this study is the degree of transcriptional similarity between developing mouse and human coronary ECs. Several groups have recently used scRNAseq to profile cell types in the fetal human heart, and identified individual genes that are enriched in either mouse or human (Asp et al., 2019; Cui et al., 2019; Miao et al., 2020; Suryawanshi et al., 2020). Here, our experiments enriched for ECs to enable a high-resolution comparison of this cellular compartment. The data showed that mouse transcriptional clusters specifically enriched in either septal or free walls cells are reproduced in our 11, 14, and 22 week human scRNAseq datasets, and many of the defining genes are conserved. Furthermore, the observation that adult human capillary ECs almost completely map to developmental Cap2 (Fig. 6c) indicates that the hypoxic and low flow Cap1 is also resolved in adult human hearts as show in mice. Although it is not possible to definitively identify the origins of human heart ECs using

scRNAseq alone, the presence of similar cell states between mouse and human at these timepoints, as well as the convergence of adult capillary cells into a single cell state in both, lends confidence to the notion that coronary development generally follows the same progression in these two species.

Despite overall similarities in cell types, the scRNAseq analysis did reveal some interesting differences in gene expression between mouse and human, some of which may explain the anatomical differences in their vasculature. For instance, human Art1 and Art2 specifically expressed the glutamate receptor *GRIA2* and the GABA receptor *GABBR2*, respectively. It was previously demonstrated that exposure of ECs to GABA *in vitro* led to a reduction in response to inflammatory stimulus (Sen et al., 2016), and that mutations in brain ECs of a different GABA receptor, *Gabrb3*, resulted in defects in neuronal development *in vivo* (Li et al., 2018). These genes were not present in adult coronary artery ECs. Further investigation may reveal an important role for GABA and glutamate signaling in human coronary development.

In summary, we have shown that in both mouse and human, phenotypically distinct lineage- and location-based cell states of coronary ECs converge into a relatively homogenous population in adults, and that embryonic lineage does not influence injury responses. This is a demonstration of the significant plasticity of the vasculature and the influence environmental factors have in shaping heterogeneity, as well as the strength of mice as a model organism for human heart development.

Methods

Mice

Mouse strains. All mouse husbandry and experiments were conducted in compliance with Stanford University Institution Animal Care and Use Committee guidelines. Mouse lines used in this study are: *BmxCreER* (Ehling et al., 2013), *ApjCreER* (Chen et al., 2014), *mTmG* (The Jackson Laboratory, *Gt(ROSA)26Sortm4(ACTB-tdTomato*,*-EGFP)Luo*/J, Stock #007576), *tdTomato* (The Jackson Laboratory, B6.Cg-Gt(ROSA)26Sortm9(CAG-*tdTomato*)Hze/J, Stock #007909), and CD1 (Charles River Laboratories, strain code: 022).

Breeding and tamoxifen administration. Timed pregnancies were determined by defining the day on which a plug was found as e0.5. For Cre inductions, Tamoxifen (Sigma-Aldrich, T5648) was dissolved in corn oil at a concentration of 20 mg/ml and 4 mg was administered to pregnant dams using the oral gavage method on days e8.5 and e9.5 (Fig 1a, Fig 3d-e, Fig S1a) or day e11.5 (Fig 1b, Fig S1c). Combined injections of tamoxifen at e8.5 and e9.5 led to labeling of 94.44% of Endo cells and 3.61% of SV cells at e12.5. For the adult injury experiments, either 4 mg of Tamoxifen or 1 mg of 4-OH Tamoxifen (Sigma-Aldrich, H6278) was delivered on day e9.5 or e10.5 (Fig 4a, Fig S1b), respectively. The five *BmxCreER-Rosa*^{tdTomato} or *ApjCreER-Rosa*^{mTmG} mice used for the scRNAseq experiment were either 8 weeks old or 20 weeks old and all female (Fig 1b). The 11 *BmxCreER-Rosa*^{tdTomato} adult mice used for the injury experiments were 12 weeks old and all male (Fig 4a). The three CD1 adult mice used for quantification of EC proliferation in uninjured hearts were 10 weeks old and all female (Fig 4e, h-i). The three CD1 adult mice used for Car4 staining were 6 weeks old and all female (Fig 3h). Adult mice for the scRNAseq and injury experiments were obtained by harvesting litters at e18.5 and fostering pups with a different female who had given birth 0-4 days earlier.

Human hearts

Under IRB approved protocols, human fetal hearts were collected for developmental analysis from elective terminations. Gestational age was determined by standard dating criteria by last menstrual period and ultrasound (Obstetrics, 2009). Tissue was processed within 1h following procedure. Tissue was extensively rinsed with cold, sterile PBS, and placed on ice in cold, sterile PBS before further processing as described below. Pregnancies complicated by multiple gestations and known fetal or chromosomal anomalies were excluded.

Single-cell RNA sequencing protocol

e12 and e17.5 mouse scRNAseq. BmxCreER-Rosa$^{tdTomato/tdTomato}$ males were crossed to CD1 females, which were dosed with tamoxifen at e8.5 and e9.5. Either early in the day on e12, or midday on e17.5, embryos were removed and placed in cold, sterile PBS. 42 Cre+ e12 embryos and 9 Cre+ e17.5 embryos were identified by their fluorescent signal and used for single-cell isolation. Hearts were isolated and dissected to remove the atria and outflow tract, keeping the ventricles, SV, and valves. Hearts were then dissociated in a 600 µl mix consisting of 500 U/ml collagenase IV (Worthington #LS004186), 1.2 U/ml dispase (Worthington #LS02100), 32 U/ml DNase I (Worthington #LS002007), and sterile DPBS with Mg2+ and Ca2+ at 37 degrees for 45 minutes and resuspended by pipetting every 5 minutes. Once digestion was complete, 5 mL of a cold 5% FBS in PBS mixture was added and the suspension was filtered through a 40 micron strainer. After further rinsing the strainer with 5 mL of 5% FBS/PBS, the cell suspension was centrifuged at 400*g* at 4°C for 5 min. The cells were washed and resuspended once more in 1 mL 5% FBS/PBS. The following antibodies were added at the concentration of 1:50 and incubated on ice for 45 minutes: APC/Cy7 Cd45 (Biolegend #103116), APC Cd31 (Biolegend #102410), APC/Cy7 Ter-119 (Biolegend #116223). DAPI (1.1 µM) was added to the cells immediately before FACS. Once stained, the cells were sorted on a Aria II SORP machine into 1.5 mL tubes. The gates were set up to sort cells with low DAPI, low Cd45 (hematopoietic cells), low Ter119

(erythroid cells), high Cd31 (endothelial marker), and either high or low PE-Texas Red (*tdTomato* positive or negative). Compensation controls were set up for each single channel (PE-Texas Red, APC, APC/Cy7) before sorting the final cells. The samples were then submitted to the Stanford Genome Sequencing Service Center for 10x single-cell v3.1 3' library preparation. For each stage, libraries from the *tdTomato* positive and negative samples were pooled and sequencing was performed on two lanes of a Illumina NovaSeq 6000 SP flow cell.

Adult mouse scRNAseq. The experiment was performed using the same procedure as e12 and e17.5 unless noted here. *BmxCreER-Rosa*$^{tdTomato/tdTomato}$ and *ApjCreER-Rosa*$^{mTmG/mTmG}$ males were crossed to CD1 females, which were dosed with tamoxifen at e11.5. Eight weeks after birth, hearts were harvested from 2 Cre+ female mice of each line and placed in cold, sterile PBS. Hearts were dissected to remove the atria, outflow tract, and valves, keeping only the ventricles. 20 weeks after birth, a heart was harvested from 1 Cre+ female *BmxCreER-Rosa*^{tdTomato} mouse. The heart was dissected to keep only the interventricular septum. Dissociation was performed as described for e12 and e17.5 except that multiple tubes of the 600 µl mix were used for each heart. The gates were set up to sort cells with low DAPI, low Cd45 (hematopoietic cells), low Ter119 (erythroid cells), high Cd31 (endothelial marker), and either high PE-Texas Red (*BmxCreER-Rosa*^{tdTomato}) or high GFP and moderate PE-TexasRed (*ApjCreER-Rosa*^{mTmG}). After staining each cell was sorted into a separate well of a 96-well plate containing 4 µl lysis buffer. Cells were spun down after sorting and stored at −80 °C until cDNA synthesis. A total of 1344 ECs from *BmxCreER-Rosa*^{tdTomato}, including 384 septal cells, and 864 ECs from *ApjCreER-Rosa*^{mTmG} were sorted and processed for cDNA synthesis. Cells were analyzed on the AATI 96-capillary fragment analyzer, and a total of 1056 cells that had sufficient cDNA concentration were barcoded and pooled for sequencing.

22 week fetal human heart scRNAseq. The experiment was performed using the same procedure as the adult mouse unless noted here. The heart was kept in cold, sterile PBS. It was dissected to remove the atria, outflow tract, and valves, keeping only the ventricles. The antibodies used for staining were: Pacific Blue CD235a (Biolegend #349107), FITC CD36 (Biolegend #336204), APC/Cy7 CD31 (Biolegend #303119), Pacific Blue CD45 (Biolegend #304021). The gates were set up to sort cells with low DAPI, low CD45 (hematopoietic cells), low CD235A (erythroid cells), high CD31 (endothelial marker), and low FITC. A total of 1920 CD31+CD36- and CD31+ cells were sorted and processed for cDNA synthesis. A total of 1382 cells that had sufficient cDNA concentration were barcoded and pooled for sequencing.

11 and 14 week fetal heart scRNAseq. The experiment was performed using the same procedure as the 22 week heart unless noted here. The antibodies used for staining were: PerCP/Cy5.5 CD235a (Biolegend #349110), PerCP/Cy5.5 CD45 (Biolegend #304028), FITC CD36 (Biolegend #336204), APC/Cy7 CD31 (Biolegend #303119). The gates were set up to sort cells with low DAPI, low CD45 (hematopoietic cells), low CD235A (erythroid cells), high CD31 (endothelial marker), and either low or high FITC. A total of 1824 CD31+CD36-, CD31+CD36+ and CD31+ cells from the 11 week heart and 1920 CD31+CD36-, CD31+CD36+ and CD31+ cells from the 14 week heart were sorted and processed for cDNA synthesis. A total of 1530 11 week and 1272 14 week cells that had sufficient cDNA concentration were barcoded and pooled for sequencing.

Synthesis of cDNA and library preparation for the adult mouse and fetal human heart cells was performed using the Smart-seq2 method as previously described (Picelli et al., 2014; Su et al., 2018). Libraries from the adult mouse and fetal human heart cells were part of a pool of samples that was sequenced on four lanes of a Illumina NovaSeq 6000 S4 flow cell.

Single-cell RNA sequencing data analysis

Processing of sequencing data. Raw Illumina reads for all datasets were demultiplexed and converted to FASTQ using *bcl2fastq* (Illumina). For adult mouse and fetal human, sequencing adapter and PCR primer sequences were trimmed from reads using cutadapt 2.7 (Martin, 2011). For e12 and e17.5, reads were aligned to GRCm38 Ensembl release 81 as well as *EGFP* and *tdTomato* sequences and a gene count matrix was obtained using Cell Ranger v3.1.0 (10X Genomics). For adult mouse and fetal human, reads were aligned with STAR v2.7.1a (Dobin et al., 2013) to GRCm38 Ensembl release 81 as well as *EGFP* and *tdTomato* sequences, and GRCh38 Ensembl release 98, respectively, and a gene count matrix was obtained using the *featureCounts* function of Subread v1.6.0 (Liao et al., 2014).

Processing of count data. The majority of scRNAseq data analysis was performed using R and Seurat v3 (Stuart et al., 2019). Cells were deemed low-quality and excluded from downstream analysis if they expressed less than 1000 genes or if more than 10% (e12, e17.5, human fetal) or more than 5% (adult mouse) of reads aligned to mitochondrial genes. A small number of cells were removed from the e17.5 *tdTomato* negative sample which were expressing *tdTomato*. For all datasets, non-endothelial subtypes (e.g. blood and immune cells, cardiomyocytes, smooth muscle, fibroblasts) as well as a small number of lymphatic cells were removed. For the adult mouse, endocardial cells were removed, as well as a cluster of cells enriched in dissociation-induced genes (ex. *Hspa1a, Hspa1b, Socs3, Junb, Atf3*) (van den Brink et al., 2017). To obtain the subsets of vascular ECs shown in Fig 1, SV, valve, endocardium, SV, and cycling cells were removed as shown in Fig S2b. Additionally, a cluster of cells with a lower gene count and higher mitochondrial percentage were removed from the e17.5 dataset. The cells used for the cell cycle analysis in Fig S4 include all the cells used Fig 1F combined with the non-endocardial cycling cells shown in Fig S2b.

Count data from Kalucka et al (Kalucka et al., 2020), Su et al (Su et al., 2018), and Litvinukova et al (Litvinukova et al., 2020) were used to analyze gene expression in adult mouse, e12.5 mouse, and adult human hearts, respectively. From these datasets only vascular endothelial cells were retained, excluding endocardium, SV, valve endothelium, lymphatic endothelium, and non-endothelial cell types.

Normalization, variable feature selection, scaling, and dimensionality reduction using principal component analysis were performed using the standard Seurat v3 pipeline (Stuart et al., 2019). For the e17.5 and adult mouse datasets the technical variables genes per cell, reads per cell, and mitochondrial read percentage were regressed out in the *ScaleData* function. Following this, construction of a shared nearest neighbor graph, cluster identification with the Louvain algorithm (Stuart et al., 2019), and Uniform Manifold Approximation and Projection (UMAP) dimensionality reduction (Becht et al., 2018) were performed using the *FindNeighbors*, *FindClusters*, and *RunUMAP* functions in Seurat using the following parameters:

Fig S2a (11520 cells)- 25 dimensions, Louvain resolution = 0.8

Fig S2b (12,205 cells)- 25 dimensions, Louvain resolution = 0.8

Fig 1c (436 cells)- 25 dimensions, Louvain resolution = 0.6

Fig 1f (4801 cells)- 25 dimensions, Louvain resolution = 0.4

Fig 1i (649 cells)- 30 dimensions, Louvain resolution = 0.9

Fig S5a (1829 cells)- 30 dimensions, Louvain resolution = 1

Fig S7a (356 cells)- 20 dimensions, Louvain resolution = 1

Fig S4a (8495 cells)- 25 dimensions, Louvain resolution = 0.4 (after regression), Louvain resolution = 0.6 (before regression)

Fig 5b (2339 cells)- 30 dimensions, Louvain resolution= 1.4

Fig 5c (1586 cells)- 20 dimensions, Louvain resolution = 1

Fig 6c (13,476 cells)- 50 dimensions, Louvain resolution = 0.8

Differential expression testing. Differential gene expression testing was performed with the *FindMarkers* and *FindAllMarkers* functions in Seurat using the Wilcoxon Rank Sum test. Differential genes used in Figs 2,3,7, and S10 were defined using parameters logfc.threshold = 0.3, min.pct = 0.2 and filtered for p-value < 0.001.

Cell cycle regression. Cell cycle regression for Fig S4 was performed using top 100 gene markers for the cycling clusters by p-value based on Wilcoxon Rank Sum test and the vars.to.regress parameter in the Seurat *ScaleData* function.

Pearson correlation. Pearson correlation heatmaps in Figs 2e-f were created with the *heatmaply_cor* function from heatmaply (Galili et al., 2018).

Dataset reference mapping. For cross-dataset mapping in Fig 5, the *getLDS* function in biomaRt (Durinck et al., 2005; Durinck et al., 2009) was used to identify every human gene that has a corresponding mouse gene and vice versa. Genes were only retained if they had a 1:1 mapping between human and mouse. The raw counts matrix for the human fetal data (all three sages pooled) was then filtered to include only these genes, and only the cells used in Fig 5c, and a new Seurat object was created from this count matrix. Similarly the raw count matrix for the e17.5 mouse data was filtered to include only these genes, and only the cells used in Fig 1f, and a new Seurat object was created from this count matrix. Standard normalization and scaling was performed in Seurat. To perform the mappings between datasets in Figs 5e-g, 6c, and S10f, the Seurat functions *FindTransferAnchors* and *TransferData* were performed using 30 dimensions and Canonical Correlation Analysis dimensionality reduction.

Trajectory analysis. Trajectory analyses shown in Fig 6b and S11b and were performed with PAGA (Wolf et al., 2019) (filtered for edge weight greater than or equal to 0.14), RNA velocity (La Manno et al., 2018) (using the python function *veloctyto run-smartseq2*, followed by the R package velocyto.R with the function *show.velocity.on.embedding.cor* with fit.quantile = 0.05, grid.n = 20, scale = 'sqrt', arrow.scale = 3, and n= 50-100), and Slingshot (Street et al., 2018) (using the *slingshot* function with Cap2 as the starting cluster and stretch = 1)

Transcription factor enrichment. Transcription factor enrichment was performed with SCENIC (Aibar et al., 2017) using the *pyscenic* functions and the recommended pipeline (Van de Sande et al., 2020). The loom file output from SCENIC was then imported into Seurat, and the *FindAllMarkers* function with the Wilcoxon Rank Sum test was used to identify differential regulons between clusters.

Immunofluorescence and imaging

Tissue processing and antibody staining. E17.5 embryos were dissected in cold 1X PBS and fixed in 4% PFA for 1 hour at 4°C, followed by three 15 minute washes in PBS. Hearts were then dissected from the embryos. Adult mouse hearts were dissected and fixed in 4% PFA for 4-5 hours at 4°C, followed by three 15 minute washes in PBS. Hearts were dehydrated in 30% sucrose overnight at 4°C, transferred to OCT for a 1 hour incubation period, and frozen at -80°C. For each heart, the whole ventricle was cut into 20 µm thick sections which were captured on glass slides. Staining was performed by adding primary antibodies diluted in .5% PBT (.5% Triton X-100 in PBS) with .5% donkey serum to the sections and incubating overnight at 4°C. The following day the slides were washed in PBS 3 times for 10 minutes followed by a 2 hour room temperature incubation with secondary antibodies, three more 10 minute washes, and mounting with Fluoromount-G (SouthernBiotech #0100-01) and a coverslip fastened using nail polish. Human fetal hearts were fixed in 4% PFA for 24-48 hrs at 4°C, followed by three 15 minute washes

in PBS. The hearts were sequentially dehydrated in 30%, 50%, 70%, 80%, 90% and 100% ethanol, washed three times for 30 minutes in xylene, washed several times in paraffin, and finally embedded in paraffin which was allowed to harden into a block. For each heart, the whole ventricle was cut into 10 µm thick sections which were captured on glass slides.

In situ hybridization. RNA was isolated from a 23 week human fetal heart using Trizol-based dissociation followed by the RNEasy Mini Kit (Qiagen #74104). cDNA was created from this RNA using the iScript Reverse Transcription Supermix (Bio-Rad #1708840). Primers used to amplify *GJA4* are: 5'-AAACTCGAGAAGATCTCGGTGGCAGAAGA-3' and 5'-AAATCTAGACTGGAGAGGAAGCCGTAGTG-3'. Primers used to amplify *GJA5* are: 5'-AAACTCGAGAATCAGTGCCTGGAGAATGG-3' and 5'-AAATCTAGATGGTCCATGGAGACAACAGA-3'. Digoxin-linked probes were transcribed using the Roche DIG RNA Labeling Kit (Millipore Sigma #11175025910). In-situ hybridization was performed as previously described (Koop et al., 1996) with a modification to develop the fluorescent signal. Briefly, after hybridization, sections were incubated overnight at 4°C with anti-DIG POD (Millipore Sigma #11207733910). The next day, sections were washed 4x 1 hour in 1X MABT. Finally, sections were washed for 3x 10 minutes with 0.1M Borate buffer pH 8.5 and stained with bench-made tyramide (Vize et al., 2009).

Microscopy and Image Processing. Images were captured on a Zeiss LSM-700 confocal microscope. For each experiment, littermate embryos were stained together and all samples were imaged using the same laser settings. For each experiment, laser intensity was set to capture the dynamic range of the signal. Images were captured using Zen (Carl Zeiss) and processed using FIJI (NIH) and Illustrator (Adobe). Any changes to brightness and contrast were applied equally across the entire image. All imaging experiments were performed with at least three individual samples.

Antibodies. The following primary antibodies were used: anti-ERG (1:200; Abcam, ab92513), anti-Car4 (1:200; R&D, AF2414), anti-Smmhc (1:100; Proteintech, 21404-1-AP), anti-Cldn5 (1:100; Invitrogen, 35-2500). Secondary antibodies were Alexa fluor-conjugated antibodies (488, 555, 633) from Life Technologies used at 1:250.

Quantification. Quantification of Car4 (Fig 3d-e) and EdU (Fig 4e-f) was performed using the CellCounter plugin in FIJI. For e17.5 embryos, Car4, Erg, and *tdTomato* were quantified in five ROIs in each of three sections from each of three hearts. The ROIs were 510 μm x 190 μm and were positioned to maximize coverage of the septum, left ventricular wall, right ventricular wall, dorsal wall, and ventral wall. For each heart, counts were combined across the three sections. For the adult injured hearts, EdU, Erg, and *tdTomato* were quantified in 2 ROIs for each of 11 hearts at the level of the stitch (quantification from 2 ROIs was averaged), and in 1 ROI for each of 7 hearts at the apex. ROIs were 600 μm x 600 μm and were chosen to be in the region of the section with the greatest density of EdU staining, and whenever possible, to span portions of both the inner and outer myocardial wall. For uninjured controls, one ROI of 600 μm x 600 μm was chosen in both the middle of the myocardial wall of the left ventricle, and at the apex, from each of three uninjured 6 week female mouse hearts. Graphs in Figs 3 and 4 were made in Prism 8.

Statistics. In Fig 4e, paired t-tests were used to compare Endo-derived and SV-derived EC proliferation, and Welch's t-test was used to compare Endo-derived or SV-derived EC proliferation with the uninjured control. Unpaired t-tests were used for Fig 4f.

Ischemia reperfusion injury experiment

Surgery. *BmxCreER-Rosa*$^{tdTomato/tdTomato}$ males were crossed to CD1 females, which were dosed with tamoxifen e9.5 or with 4-OH tamoxifen at e10.5. In addition to being pharmacologically less

toxic compared to Tam, 4-OHT is more potent at inducing Cre, given its stronger affinity for the ER domain in *CreER* strain (Robertson et al., 1982; Katzenellenbogen et al., 1984; Cardoso et al., 2003). By administering 4-OHT 1 day later than Tam, Cre was induced in all animals at approximately the same developmental time regardless of treatment. Pups were dissected from the pregnant dams at day e18.5 and fostered as described above. Ischemia-reperfusion (IR) was performed in 12-week old mice by the Stanford Murine Phenotyping Core (SMPC) that is directed by Dr. Dan Bernstein. To summarize, mice were anesthetized using isoflurane and placed on a rodent ventilator to maintain respiration before opening the chest cavity. The left anterior descending coronary artery (LAD) was ligated with a 8.0 silk suture and resulting ischemia of the myocardium was verified by blanching the left ventricular wall. After 40 min, the suture was removed around the LAD, allowing for the reperfusion of downstream myocardium. To end the procedure, the chest was closed, and post-operative analgesia was administered to the mice.

In vivo proliferation assay. To assess EC proliferation after IR, 5-ethynyl-2′-deoxyuridine (EdU) (Thermo Fisher Scientific, cat. #E10415) was diluted 2.5 mg/ mL in sterile PBS and injected intraperitoneally on days 3 and 4 post-injury at a dose of 10 µL/ g body weight. Hearts were harvested from sacrificed animals on day 5 post-injury. Cryosectioning and antibody staining for Erg was performed as described above. To detect endothelial proliferation, the protocol for Click-iT® EdU Imaging (Thermo Fisher Scientific, cat. #C10086) was carried out according to manufacturer instructions. *BMX-CreER^{T2}; Rosa26^{tdTomat}* was observed to label ECs in large arteries in adult tissues even without tamoxifen administration (Red-Horse Lab, unpublished data). Since the developmental origin of adult arteries cannot be determined using *BMXCreER*, large arteries were excluded from all ROIs during quantification.

Acknowledgements

K.R. is supported by the NIH (R01-HL128503). R.P. is supported by an AHA graduate fellowship. Sequencing of the adult mouse and fetal human datasets was funded by the Chan Zuckerberg Biohub. We thank Ralf Adams for sharing the *BmxCreER* mouse line. We thank the Stanford Family Planning Clinic and Purnima Iyer Narasimhan for assistance with tissue procurement. We thank Gavin Sherlock for access to equipment needed for single-cell library preparation. We thank all members of the Red-Horse lab for technical and intellectual support. We thank Rahul Sinha, Anshul Kundaje and Laksshman Sundaram for discussion and advice about scRNAseq technique and analysis. We thank Biafra Ahanonu for discussion and advice about figure and manuscript preparation. We thank members of the Stanford Genome Sequencing Services Center which is supported by NIH Grant # 1S10OD020141-01. V.D.W. is supported by the H&H Evergreen Fund.

Contributions

R.P., G.D., and K.R. conceptualized the study and wrote the manuscript. R.P. and G.D. performed experiments. R.P., J.K. and M.Z. performed cardiac injury study. R.P. performed computational analysis. S.S.K., R.C.J., S.R.Q., I.W., V.D.W., and D.B. assisted with experiments and provided experimental resources.

Figure Legends

Figure 1: ScRNAseq of lineage-traced coronary ECs at three stages reveals capillary heterogeneity during embryonic development. (A and B) Overview of lineage tracing and scRNAseq approach in embryonic (A) and adult (B) mice. (C-H) Unbiased clustering of embryonic coronary ECs at the indicated time points and the contribution of Endo-enriched (*BmxCreER* lineage-labeled) and SV-enriched (*BmxCreER* lineage negative) cells to each cluster. UMAPs are shown for combined data (C and F) and separated by lineage (D and G) and percentages enumerated (E and H). (I-K) Combined (I) and separated (J) UMAPs and clusters for adult coronary ECs. Endo-enriched are *BmxCreER* lineage-labeled, SV-enriched are *ApjCreER* lineage-labeled. (K) Percentages of cells per cluster.

Figure 2: Expression of Endo and SV genes in coronary ECs. (A) Heatmap showing expression of the top 30 (by p-value) Endo-defining genes (enriched in the Endo compared to the SV) and the top 30 (by p-value) SV-defining genes (enriched in the SV compared to the Endo) in e12 and e17.5 capillary clusters (E = coronary cells from the Endo-enriched sample, S = coronary cells from the SV-enriched sample). (B and C) Venn-diagrams showing overlap of Endo- and SV-defining genes with Cap1 enriched genes (enriched in Cap1 compared to Cap2) and e12 Cap2 enriched genes (enriched in Cap2 compared to Cap1) at e12 (B) and e17.5 (C). (D) Venn-diagram showing overlap of e12 Cap1 and Cap2 enriched genes with e17.5 Cap1 and Cap2 genes. (E and F) Heatmaps of Pearson correlations based on expression of Endo- and SV-defining genes in the Endo, the SV, and capillary clusters from e12 and e17.5 in total (E) and separated by *BmxCreER* lineage as indicated by *tdTomato* (*td*) expression (F). G) Venn-diagram showing overlap of adult Cap2 enriched genes (enriched in Cap2 compared to Cap1) with the indicated categories.

Figure 3: Gene expression and localization of e17.5 capillary clusters. (A) Heatmap showing expression of selected genes enriched in either Cap1 or Cap2 at e17.5 (E = coronary cells from Endo-enriched sample, S = coronary cells from SV-enriched sample). (B) UMAPs showing expression of selected flow-induced, hypoxia-induced, and tip-cell genes. Dashed lines outline indicated clusters. (C) *Car4* UMAPs separated by lineage. Dashed line shows area of UMAP enriched in Endo-derived, *Car4*-negative cells predicted to be located in the septum. (D) Immunofluorescence of Car4 and Erg in a heart section from an e17.5 *BmxCreER;Rosa*^{tdTomato} embryo (scale bar = 500 μm). Red arrows indicate Car4-positive, tdTomato-positive Endo-derived ECs in the dorsal wall. (E) Quantification of Car4 staining in *Erg*-positive cells from three e17.5 *BmxCreER;Rosa*^{tdTomato} embryos (error bars = SD). (F) Images showing in-situ hybridization for *Kcne3* in an e14.5 embryonic mouse heart, obtained from GenePaint. (G) UMAPs showing cells in the adult scRNA-seq dataset isolated from the septum-only sample, and expression of *Car4* in adult coronary ECs (scale bar = 100 μm). (H) Immunofluorescence of Car4 and Erg in the left ventricle (LV) and septum of an adult WT heart. (I) Schematic illustrating convergence of Endo- and SV-derived ECs into equivalent transcriptional states. Scale bar from (B) also applies to (C), (F), and (G).

Figure 4: Comparison of injury responses of Endo- and SV-derived coronary ECs. (A) Overview of lineage tracing and ischemia-reperfusion (I/R) injury approach in adult mice. (B) Example of how EdU localization highlights mid-myocardial injury region. Yellow arrowheads indicate the injury region with dense EdU staining. (C and D) Immunofluorescence of EdU and Erg in sections of the heart from (B) just below level of the stitch (C) and in the apex (D). Yellow arrowheads show proliferating Endo-derived ECs that are positive for tdTomato, Erg, and EdU; white arrowheads show tdTomato-negative, Erg-positive ECs from the SV that are EdU positive. (E) Quantification in multiple injured hearts of EdU-positive, Erg-positive ECs from the two

lineages. (F) Quantification in multiple injured hearts of EdU-positive, Erg-positive ECs from the inner and outer wall, both in the focal area of the injury, as indicated in (B), and in areas adjacent to the injury. Scale bars = 500 μm.

Figure 5: ScRNAseq of coronary ECs from human fetal hearts. (A) Overview of scRNAseq approach for three human fetal hearts. (B and C) UMAPs of all major *Pecam1*+ EC subtypes collected (B) and the non-cycling coronary EC subset (C). (D) Pie charts showing the breakdown by cluster of human coronary ECs that were sorted as *CD31*+ without additional enrichment. (E) Schematic of inter-species reference mapping. Individual cells from the human or mouse e17.5 datasets were assigned to the most similar mouse or human cluster, respectively. (F and G) Results from inter-species reference mapping based on shared gene expression, showing the mouse cluster that each human EC mapped to and the percentage breakdown of the mapping from each human cluster (F) and the converse comparison (G). Dashed lines show the borders of the previously defined human and mouse e17.5 coronary clusters. (H) UMAPs showing expression of selected flow-induced, hypoxia-induced and tip-cell genes in human coronary ECs. (I) Schematic illustrating enrichment of septum ECs in mouse Cap1 and human Cap1 and Art3, as well as trajectories from capillary to artery in both human and mouse.

Figure 6: Trajectory analysis of developing human coronary arteries. (A) Reference mapping showed that e17.5 mouse ECs from Fig 5G were assigned to all three human artery subsets. (B) Trajectory analysis of human coronary ECs using PAGA, Slingshot, and RNA velocity suggested that artery ECs are formed by capillary EC differentiation, as in mice. (C) Reference mapping adult human coronary ECs from a publicly available dataset to human fetal ECs showed that most mature cells match to Art1, Art2 or Cap2. (D) UMAPs showing expression of selected genes shared between hCap1 and hArt3 and hCap2 and hArt2, in both human and mouse. Previously defined clusters are outlined.

Figure 7: Gene expression in developing human coronary arteries. (A) Heatmap showing expression of selected genes enriched in human artery clusters. (B and C) Regulon scores from *SCENIC* analysis for TFs enriched in all human and mouse artery clusters (B) and for TFs enriched in human and mouse Art1 (C). (D) Human, but not mouse, developing coronary arteries expressed neurotransmitter receptors and their transporter. (E) *GJA4* and *GJA5* expression in human coronary ECs. (F) Serial sections from 18wk human fetal heart showing *in-situ* hybridization for the indicated mRNAs with immunofluorescence for the indicated proteins.
Cluster hArt1 (*GJA5+GJA4+*) localizes to the largest arteries that are covered by mature SMMHC-positive smooth muscle (white arrows). Clusters hArt2 and 3 (*GJA4-GJA4+*) are smaller and can be either covered (yellow arrowheads) or not (red arrowheads) by smooth muscle. Scale bar = 100 µm. Scale bar from (E) also applies to (D).

Supplementary Figure 1: Localization and expression of recombinant markers. (A and B) *tdTomato* localization in sections *BmxCreER;Rosa*^{tdTomato} hearts at e17.5 (A) and adult (B). (C) *GFP* localization in a section an *ApjCreER;Rosa*^{mTmG} adult heart. (D and E) Expression of the *tdTomato* gene in the Endo-enriched (Endo lineage pos) and SV-enriched (Endo lineage neg) sorted samples at e12 (D) and e17.5 (E) from *BmxCreER;Rosa*^{tdTomato} hearts (as shown in Fig 1a). (F and G) Expression of the *tdTomato* and *GFP* genes in the SV lineage negative and SV lineage positive sorted cells from adult *ApjCreER;Rosa*^{mTmG} hearts, and in the Endo lineage negative and Endo lineage positive sorted cells from adult *BmxCreER;Rosa*^{tdTomato} adult hearts (as shown in Fig 1b). Scale bars = 500 µm.

Supplementary Figure 2: Selection of coronary vascular ECs from e12 and e17.5 datasets. **(**A and B) UMAPs showing expression of selected EC subtype markers in e12 ECs (A) and e17.5 ECs (B). (C and D) UMAPs showing the cells that were used for the analysis of e12 coronary ECs

in Fig 1c (C) and for the analysis of e17.5 coronary ECs in Fig 1f (D). Scale bar from (A) also applies to (B) and (C).

Supplementary Figure 3: Coronary EC subtype markers. (A, B and C) UMAPs showing expression of selected coronary EC subtype markers in coronary ECs at e12 (A), e17.5 (B) and adult (C). Scale bar from (C) also applies to (A) and (B).

Supplementary Figure 4: Cell cycle regression in e17.5 coronary ECs. (A) UMAP showing unbiased clustering of e17.5 mouse coronary ECs before the removal of cycling cells. (B) UMAP showing unbiased clustering of e17.5 mouse coronary ECs from (A) after cell cycle regression was performed. (C) Post-regression UMAP from (B) showing the cycling cells which were in the cycling cluster in (A). (D) Breakdown of Endo- and SV-enriched cells from (B) by cluster. (E) Breakdown of the capillary clusters in (B) into cells that are cycling or non-cycling.

Supplementary Figure 5: Analysis of an additional adult mouse coronary EC dataset. (A) UMAP showing unbiased clustering of coronary ECs from a previously published adult dataset (Kalucka et al., 2020). (B) UMAPs showing expression of selected coronary EC subtype markers. (C) Expression of *Apln* in the adult coronary EC dataset from Fig 1, broken down into SV lineage negative (GFP_neg) and SV lineage positive (GFP_pos) cells from *ApjCreER;Rosa*^{mTmG} hearts, and Endo lineage negative (Td_neg) and Endo lineage positive (Td_pos) cells from *BmxCreER;Rosa*^{tdTomato} hearts. Scale bar from (B) also applies to (C).

Supplementary Figure 6: Expression of selected Endo- and SV-defining genes. (A) UMAP showing expression of canonical Endo (*Cdh11*) and SV (*Vwf, Bmp4*) markers in heart ECs at e12. (B, C and D) Expression of genes enriched in either the Endo (Endo-defining genes) or the SV

(SV-defining genes) in all e12 ECs (B), e12 coronary plexus ECs (C) and e17.5 coronary ECs (D). Scale bar from (A) also applies to (B), (C), and (D).

Supplementary Figure 7: Expression of e12 Cap1- and Cap2-specific genes in a dataset of e12.5 SV-derived ECs. (A) UMAP showing expression of selected coronary EC subtype markers in a previously published dataset (Su et al., 2018). (B and C) Expression in e12 dataset of genes enriched in e12 Cap1 (B) or Cap2 (C). (D and E) Expression in Su *et al.* dataset of genes enriched in e12 Cap1 (D) or Cap2 (E). Scale bar from (A) also applies to (B), (C), (D), and (E).

Supplementary Figure 8: Expression of flow-induced genes. (A) UMAPs showing expression of selected flow-induced genes from Kumar et al 2014 (Kumar et al., 2014) in e17.5 coronary ECs.

Supplementary Figure 9: Expression of Endo- and SV-defining genes at e17.5. (A) UMAPs showing expression of Endo-enriched genes manually determined to be expressed in a higher percentage of putative septum cells (as shown in Fig 3c) than non-septum cells. (B) UMAPs showing expression of SV-enriched genes manually determined to be expressed in a higher percentage of non-septum cells than septum cells. C) UMAPs showing expression of SV-enriched genes manually determined to be expressed in a higher percentage of Cap2 cells compared to Cap1 cells. Starred genes are significantly differentially expressed between e17.5 Cap1 and Cap2, as indicated in Fig 2C. Scale bar from (B) also applies to (A) and (C).

Supplementary Figure 10: Additional analysis of developing human coronary ECs. (A) Immunofluorescence for *CD36* and *Erg* in a section from a 14 wk human fetal heart. (B) UMAPs showing expression of *CD36* in human coronary ECs as well as cells colored according to FACS sample, i.e. *CD31*+ only, *CD31*+*CD36*+, *CD31*+*CD36*-, as indicated in Fig 5a. Dashed lines show

the borders of the previously defined human coronary clusters. (C) Dot plot showing the expression of selected gene markers for each human EC cluster from Fig 5b. (D) UMAPs showing expression of selected genes with shared expression patterns between mouse e17.5 and human fetal capillary ECs. (E) UMAPs showing mouse e17.5 coronary EC clusters including a manually-defined septum cluster as shown in Fig 3c, and the fetal human coronary ECs which map to each of these clusters. (F) UMAPs showing expression of selected capillary and artery genes in adult human coronary ECs from a previously published dataset (Litvinukova et al., 2020). (G) UMAPs showing expression of selected genes shared between human Cap1 and Art3 or between human Cap2 and Art2. Scale bar from (B) also applies to (D), (F), and (G).

Supplementary Figure 11: Analysis of developing human coronary ECs separated by stage. (A) UMAPs showing unbiased clustering of cells isolated from each individual human fetal heart. (B) Trajectory analysis of human coronary EC at each individual stage using RNA velocity, PAGA, Slingshot, and Monocle.

References

Aibar, S., Gonzalez-Blas, C.B., Moerman, T., Huynh-Thu, V.A., Imrichova, H., Hulselmans, G., Rambow, F., Marine, J.C., Geurts, P., Aerts, J.*, et al.* (2017). SCENIC: single-cell regulatory network inference and clustering. Nat Methods *14*, 1083-1086.

Anisimova, A.S., Meerson, M.B., Gerashchenko, M.V., Kulakovskiy, I.V., Dmitriev, S.E., and Gladyshev, V.N. (2020). Multifaceted deregulation of gene expression and protein synthesis with age. Proc Natl Acad Sci U S A *117*, 15581-15590.

Arita, Y., Nakaoka, Y., Matsunaga, T., Kidoya, H., Yamamizu, K., Arima, Y., Kataoka-Hashimoto, T., Ikeoka, K., Yasui, T., Masaki, T.*, et al.* (2014). Myocardium-derived angiopoietin-1 is essential for coronary vein formation in the developing heart. Nat Commun *5*, 4552.

Asp, M., Giacomello, S., Larsson, L., Wu, C., Furth, D., Qian, X., Wardell, E., Custodio, J., Reimegard, J., Salmen, F.*, et al.* (2019). A Spatiotemporal Organ-Wide Gene Expression and Cell Atlas of the Developing Human Heart. Cell *179*, 1647-1660 e1619.

Becht, E., McInnes, L., Healy, J., Dutertre, C.A., Kwok, I.W.H., Ng, L.G., Ginhoux, F., and Newell, E.W. (2018). Dimensionality reduction for visualizing single-cell data using UMAP. Nat Biotechnol.

Cardoso, C.M., Moreno, A.J., Almeida, L.M., and Custodio, J.B. (2003). Comparison of the changes in adenine nucleotides of rat liver mitochondria induced by tamoxifen and 4-hydroxytamoxifen. Toxicol In Vitro *17*, 663-670.

Chen, H.I., Sharma, B., Akerberg, B.N., Numi, H.J., Kivela, R., Saharinen, P., Aghajanian, H., McKay, A.S., Bogard, P.E., Chang, A.H.*, et al.* (2014). The sinus venosus contributes to coronary vasculature through VEGFC-stimulated angiogenesis. Development *141*, 4500-4512.

Corada, M., Orsenigo, F., Morini, M.F., Pitulescu, M.E., Bhat, G., Nyqvist, D., Breviario, F., Conti, V., Briot, A., Iruela-Arispe, M.L.*, et al.* (2013). Sox17 is indispensable for acquisition and maintenance of arterial identity. Nat Commun *4*, 2609.

Cui, Y., Zheng, Y., Liu, X., Yan, L., Fan, X., Yong, J., Hu, Y., Dong, J., Li, Q., Wu, X.*, et al.* (2019). Single-Cell Transcriptome Analysis Maps the Developmental Track of the Human Heart. Cell Rep *26*, 1934-1950 e1935.

Dekker, R.J., van Soest, S., Fontijn, R.D., Salamanca, S., de Groot, P.G., VanBavel, E., Pannekoek, H., and Horrevoets, A.J. (2002). Prolonged fluid shear stress induces a distinct set of endothelial cell genes, most specifically lung Kruppel-like factor (KLF2). Blood *100*, 1689-1698.

del Toro, R., Prahst, C., Mathivet, T., Siegfried, G., Kaminker, J.S., Larrivee, B., Breant, C., Duarte, A., Takakura, N., Fukamizu, A.*, et al.* (2010). Identification and functional analysis of endothelial tip cell-enriched genes. Blood *116*, 4025-4033.

Dick, S.A., Macklin, J.A., Nejat, S., Momen, A., Clemente-Casares, X., Althagafi, M.G., Chen, J., Kantores, C., Hosseinzadeh, S., Aronoff, L.*, et al.* (2019). Self-renewing resident cardiac macrophages limit adverse remodeling following myocardial infarction. Nat Immunol *20*, 29-39.

Dobin, A., Davis, C.A., Schlesinger, F., Drenkow, J., Zaleski, C., Jha, S., Batut, P., Chaisson, M., and Gingeras, T.R. (2013). STAR: ultrafast universal RNA-seq aligner. Bioinformatics *29*, 15-21.

Durinck, S., Moreau, Y., Kasprzyk, A., Davis, S., De Moor, B., Brazma, A., and Huber, W. (2005). BioMart and Bioconductor: a powerful link between biological databases and microarray data analysis. Bioinformatics *21*, 3439-3440.

Durinck, S., Spellman, P.T., Birney, E., and Huber, W. (2009). Mapping identifiers for the integration of genomic datasets with the R/Bioconductor package biomaRt. Nat Protoc *4*, 1184-1191.

Ehling, M., Adams, S., Benedito, R., and Adams, R.H. (2013). Notch controls retinal blood vessel maturation and quiescence. Development *140*, 3051-3061.

Fernandez, B., Duran, A.C., Fernandez, M.C., Fernandez-Gallego, T., Icardo, J.M., and Sans-Coma, V. (2008). The coronary arteries of the C57BL/6 mouse strains: implications for comparison with mutant models. J Anat *212*, 12-18.

Galili, T., O'Callaghan, A., Sidi, J., and Sievert, C. (2018). heatmaply: an R package for creating interactive cluster heatmaps for online publishing. Bioinformatics *34*, 1600-1602.

Gerber, T., Murawala, P., Knapp, D., Masselink, W., Schuez, M., Hermann, S., Gac-Santel, M., Nowoshilow, S., Kageyama, J., Khattak, S.*, et al.* (2018). Single-cell analysis uncovers convergence of cell identities during axolotl limb regeneration. Science *362*.

Gonzalez-Hernandez, S., Gomez, M.J., Sanchez-Cabo, F., Mendez-Ferrer, S., Munoz-Canoves, P., and Isern, J. (2020). Sox17 Controls Emergence and Remodeling of Nestin-Expressing Coronary Vessels. Circ Res *127*, e252-e270.

Gulati, G.S., Sikandar, S.S., Wesche, D.J., Manjunath, A., Bharadwaj, A., Berger, M.J., Ilagan, F., Kuo, A.H., Hsieh, R.W., Cai, S.*, et al.* (2020). Single-cell transcriptional diversity is a hallmark of developmental potential. Science *367*, 405-411.

Hamik, A., Lin, Z., Kumar, A., Balcells, M., Sinha, S., Katz, J., Feinberg, M.W., Gerzsten, R.E., Edelman, E.R., and Jain, M.K. (2007). Kruppel-like factor 4 regulates endothelial inflammation. J Biol Chem *282*, 13769-13779.

He, L., Tian, X., Zhang, H., Wythe, J.D., and Zhou, B. (2014). Fabp4-CreER lineage tracing reveals two distinctive coronary vascular populations. J Cell Mol Med *18*, 2152-2156.

Hellstrom, M., Phng, L.K., Hofmann, J.J., Wallgard, E., Coultas, L., Lindblom, P., Alva, J., Nilsson, A.K., Karlsson, L., Gaiano, N.*, et al.* (2007). Dll4 signalling through Notch1 regulates formation of tip cells during angiogenesis. Nature *445*, 776-780.

Heng, J.S., Rattner, A., Stein-O'Brien, G.L., Winer, B.L., Jones, B.W., Vernon, H.J., Goff, L.A., and Nathans, J. (2019). Hypoxia tolerance in the Norrin-deficient retina and the chronically hypoxic brain studied at single-cell resolution. Proc Natl Acad Sci U S A *116*, 9103-9114.

Kalucka, J., de Rooij, L., Goveia, J., Rohlenova, K., Dumas, S.J., Meta, E., Conchinha, N.V., Taverna, F., Teuwen, L.A., Veys, K.*, et al.* (2020). Single-Cell Transcriptome Atlas of Murine Endothelial Cells. Cell *180*, 764-779 e720.

Katzenellenbogen, B.S., Norman, M.J., Eckert, R.L., Peltz, S.W., and Mangel, W.F. (1984). Bioactivities, estrogen receptor interactions, and plasminogen activator-inducing activities of tamoxifen and hydroxy-tamoxifen isomers in MCF-7 human breast cancer cells. Cancer Res *44*, 112-119.

Keleg, S., Kayed, H., Jiang, X., Penzel, R., Giese, T., Buchler, M.W., Friess, H., and Kleeff, J. (2007). Adrenomedullin is induced by hypoxia and enhances pancreatic cancer cell invasion. Int J Cancer *121*, 21-32.

Konstantinides, N., Kapuralin, K., Fadil, C., Barboza, L., Satija, R., and Desplan, C. (2018). Phenotypic Convergence: Distinct Transcription Factors Regulate Common Terminal Features. Cell *174*, 622-635 e613.

Koop, K.E., MacDonald, L.M., and Lobe, C.G. (1996). Transcripts of Grg4, a murine groucho-related gene, are detected in adjacent tissues to other murine neurogenic gene homologues during embryonic development. Mech Dev *59*, 73-87.

Krishnan, A., Samtani, R., Dhanantwari, P., Lee, E., Yamada, S., Shiota, K., Donofrio, M.T., Leatherbury, L., and Lo, C.W. (2014). A detailed comparison of mouse and human cardiac development. Pediatr Res *76*, 500-507.

Kumar, D., Hacker, T.A., Buck, J., Whitesell, L.F., Kaji, E.H., Douglas, P.S., and Kamp, T.J. (2005). Distinct mouse coronary anatomy and myocardial infarction consequent to ligation. Coron Artery Dis *16*, 41-44.

Kumar, S., Kim, C.W., Son, D.J., Ni, C.W., and Jo, H. (2014). Flow-dependent regulation of genome-wide mRNA and microRNA expression in endothelial cells in vivo. Sci Data *1*, 140039.

La Manno, G., Soldatov, R., Zeisel, A., Braun, E., Hochgerner, H., Petukhov, V., Lidschreiber, K., Kastriti, M.E., Lonnerberg, P., Furlan, A.*, et al.* (2018). RNA velocity of single cells. Nature *560*, 494-498.

Lee, W.H., Wang, G.M., Yang, X.L., Seaman, L.B., and Vannucci, S.I. (1999). Perinatal hypoxia-ischemia decreased neuronal but increased cerebral vascular endothelial IGFBP3 expression. Endocrine *11*, 181-188.

Li, H., Horns, F., Wu, B., Xie, Q., Li, J., Li, T., Luginbuhl, D.J., Quake, S.R., and Luo, L. (2017). Classifying Drosophila Olfactory Projection Neuron Subtypes by Single-Cell RNA Sequencing. Cell *171*, 1206-1220 e1222.

Li, S., Kumar, T.P., Joshee, S., Kirschstein, T., Subburaju, S., Khalili, J.S., Kloepper, J., Du, C., Elkhal, A., Szabo, G.*, et al.* (2018). Endothelial cell-derived GABA signaling modulates neuronal migration and postnatal behavior. Cell Res *28*, 221-248.

Liao, Y., Smyth, G.K., and Shi, W. (2014). featureCounts: an efficient general purpose program for assigning sequence reads to genomic features. Bioinformatics *30*, 923-930.

Litvinukova, M., Talavera-Lopez, C., Maatz, H., Reichart, D., Worth, C.L., Lindberg, E.L., Kanda, M., Polanski, K., Heinig, M., Lee, M.*, et al.* (2020). Cells of the adult human heart. Nature *588*, 466-472.

Liu, Q., Hu, T., He, L., Huang, X., Tian, X., Zhang, H., He, L., Pu, W., Zhang, L., Sun, H.*, et al.* (2015). Genetic targeting of sprouting angiogenesis using Apln-CreER. Nat Commun *6*, 6020.

Luecken, M.D., and Theis, F.J. (2019). Current best practices in single-cell RNA-seq analysis: a tutorial. Mol Syst Biol *15*, e8746.

Marques, S., van Bruggen, D., Vanichkina, D.P., Floriddia, E.M., Munguba, H., Varemo, L., Giacomello, S., Falcao, A.M., Meijer, M., Bjorklund, A.K.*, et al.* (2018). Transcriptional Convergence of Oligodendrocyte Lineage Progenitors during Development. Dev Cell *46*, 504-517 e507.

Martin, M. (2011). Cutadapt removes adapter sequences from high-throughput sequencing reads. EMBnetjournal *17*, 10-12.

Merz, S.F., Korste, S., Bornemann, L., Michel, L., Stock, P., Squire, A., Soun, C., Engel, D.R., Detzer, J., Lorchner, H.*, et al.* (2019). Contemporaneous 3D characterization of acute and chronic myocardial I/R injury and response. Nat Commun *10*, 2312.

Miao, Y., Tian, L., Martin, M., Paige, S.L., Galdos, F.X., Li, J., Klein, A., Zhang, H., Ma, N., Wei, Y.*, et al.* (2020). Intrinsic Endocardial Defects Contribute to Hypoplastic Left Heart Syndrome. Cell Stem Cell *27*, 574-589 e578.

Miquerol, L., Langille, B.L., and Nagy, A. (2000). Embryonic development is disrupted by modest increases in vascular endothelial growth factor gene expression. Development *127*, 3941-3946.

Obstetrics, A. (2009). ACOG practice bulletin no. 107: induction of labor. Obstet Gynecol *114*, 386-397
.

Payne, S., Gunadasa-Rohling, M., Neal, A., Redpath, A.N., Patel, J., Chouliaras, K.M., Ratnayaka, I., Smart, N., and De Val, S. (2019). Regulatory pathways governing murine coronary vessel formation are dysregulated in the injured adult heart. Nat Commun *10*, 3276.

Picelli, S., Faridani, O.R., Bjorklund, A.K., Winberg, G., Sagasser, S., and Sandberg, R. (2014). Full-length RNA-seq from single cells using Smart-seq2. Nat Protoc *9*, 171-181.

Red-Horse, K., Ueno, H., Weissman, I.L., and Krasnow, M.A. (2010). Coronary arteries form by developmental reprogramming of venous cells. Nature *464*, 549-553.

Robertson, D.W., Katzenellenbogen, J.A., Long, D.J., Rorke, E.A., and Katzenellenbogen, B.S. (1982). Tamoxifen antiestrogens. A comparison of the activity, pharmacokinetics, and metabolic activation of the cis and trans isomers of tamoxifen. J Steroid Biochem *16*, 1-13.

Sathe, P., Vremec, D., Wu, L., Corcoran, L., and Shortman, K. (2013). Convergent differentiation: myeloid and lymphoid pathways to murine plasmacytoid dendritic cells. Blood *121*, 11-19.

Sen, S., Roy, S., Bandyopadhyay, G., Scott, B., Xiao, D., Ramadoss, S., Mahata, S.K., and Chaudhuri, G. (2016). gamma-Aminobutyric Acid Is Synthesized and Released by the Endothelium: Potential Implications. Circ Res *119*, 621-634.

Sharma, B., Ho, L., Ford, G.H., Chen, H.I., Goldstone, A.B., Woo, Y.J., Quertermous, T., Reversade, B., and Red-Horse, K. (2017). Alternative Progenitor Cells Compensate to Rebuild the Coronary Vasculature in Elabela- and Apj-Deficient Hearts. Dev Cell *42*, 655-666 e653.

Simons, D., Grieb, G., Hristov, M., Pallua, N., Weber, C., Bernhagen, J., and Steffens, G. (2011). Hypoxia-induced endothelial secretion of macrophage migration inhibitory factor and role in endothelial progenitor cell recruitment. J Cell Mol Med *15*, 668-678.

Smart, N. (2017). Prospects for improving neovascularization of the ischemic heart: Lessons from development. Microcirculation *24*.

Sorop, O., van de Wouw, J., Chandler, S., Ohanyan, V., Tune, J.D., Chilian, W.M., Merkus, D., Bender, S.B., and Duncker, D.J. (2020). Experimental animal models of coronary microvascular dysfunction. Cardiovasc Res *116*, 756-770.

Street, K., Risso, D., Fletcher, R.B., Das, D., Ngai, J., Yosef, N., Purdom, E., and Dudoit, S. (2018). Slingshot: cell lineage and pseudotime inference for single-cell transcriptomics. BMC Genomics *19*, 477.

Stuart, T., Butler, A., Hoffman, P., Hafemeister, C., Papalexi, E., Mauck, W.M., 3rd, Hao, Y., Stoeckius, M., Smibert, P., and Satija, R. (2019). Comprehensive Integration of Single-Cell Data. Cell *177*, 1888-1902 e1821.

Su, T., Stanley, G., Sinha, R., D'Amato, G., Das, S., Rhee, S., Chang, A.H., Poduri, A., Raftrey, B., Dinh, T.T.*, et al.* (2018). Single-cell analysis of early progenitor cells that build coronary arteries. Nature *559*, 356-362.

Suryawanshi, H., Clancy, R., Morozov, P., Halushka, M.K., Buyon, J.P., and Tuschl, T. (2020). Cell atlas of the foetal human heart and implications for autoimmune-mediated congenital heart block. Cardiovasc Res *116*, 1446-1457.

Tazuke, S.I., Mazure, N.M., Sugawara, J., Carland, G., Faessen, G.H., Suen, L.F., Irwin, J.C., Powell, D.R., Giaccia, A.J., and Giudice, L.C. (1998). Hypoxia stimulates insulin-like growth factor binding protein 1 (IGFBP-1) gene expression in HepG2 cells: a possible model for IGFBP-1 expression in fetal hypoxia. Proc Natl Acad Sci U S A *95*, 10188-10193.

Tian, X., Hu, T., Zhang, H., He, L., Huang, X., Liu, Q., Yu, W., He, L., Yang, Z., Yan, Y.*, et al.* (2014). Vessel formation. De novo formation of a distinct coronary vascular population in neonatal heart. Science *345*, 90-94.

Tomi, M., Tajima, A., Tachikawa, M., and Hosoya, K. (2008). Function of taurine transporter (Slc6a6/TauT) as a GABA transporting protein and its relevance to GABA transport in rat retinal capillary endothelial cells. Biochim Biophys Acta *1778*, 2138-2142.

Van de Sande, B., Flerin, C., Davie, K., De Waegeneer, M., Hulselmans, G., Aibar, S., Seurinck, R., Saelens, W., Cannoodt, R., Rouchon, Q.*, et al.* (2020). A scalable SCENIC workflow for single-cell gene regulatory network analysis. Nat Protoc *15*, 2247-2276.

van den Brink, S.C., Sage, F., Vertesy, A., Spanjaard, B., Peterson-Maduro, J., Baron, C.S., Robin, C., and van Oudenaarden, A. (2017). Single-cell sequencing reveals dissociation-induced gene expression in tissue subpopulations. Nat Methods *14*, 935-936.

Vize, P.D., McCoy, K.E., and Zhou, X. (2009). Multichannel wholemount fluorescent and fluorescent/chromogenic in situ hybridization in Xenopus embryos. Nat Protoc *4*, 975-983.

Wang, J., and Zhang, S. (2020). Fluid shear stress modulates endothelial inflammation by targeting LIMS2. Exp Biol Med (Maywood) *245*, 1656-1663.

Wei, K., Diaz-Trelles, R., Liu, Q., Diez-Cunado, M., Scimia, M.C., Cai, W., Sawada, J., Komatsu, M., Boyle, J.J., Zhou, B.*, et al.* (2015). Developmental origin of age-related coronary artery disease. Cardiovasc Res *107*, 287-294.

Weinreb, C., Rodriguez-Fraticelli, A., Camargo, F.D., and Klein, A.M. (2020). Lineage tracing on transcriptional landscapes links state to fate during differentiation. Science *367*.

Wessels, A., and Sedmera, D. (2003). Developmental anatomy of the heart: a tale of mice and man. Physiol Genomics *15*, 165-176.

Wolf, F.A., Hamey, F.K., Plass, M., Solana, J., Dahlin, J.S., Gottgens, B., Rajewsky, N., Simon, L., and Theis, F.J. (2019). PAGA: graph abstraction reconciles clustering with trajectory inference through a topology preserving map of single cells. Genome Biol *20*, 59.

Wu, B., Zhang, Z., Lui, W., Chen, X., Wang, Y., Chamberlain, A.A., Moreno-Rodriguez, R.A., Markwald, R.R., O'Rourke, B.P., Sharp, D.J.*, et al.* (2012). Endocardial cells form the coronary arteries by angiogenesis through myocardial-endocardial VEGF signaling. Cell *151*, 1083-1096.

Yamanaka, S. (2020). Pluripotent Stem Cell-Based Cell Therapy-Promise and Challenges. Cell Stem Cell *27*, 523-531.

Zeini, M., Hang, C.T., Lehrer-Graiwer, J., Dao, T., Zhou, B., and Chang, C.P. (2009). Spatial and temporal regulation of coronary vessel formation by calcineurin-NFAT signaling. Development *136*, 3335-3345.

Zhang, H., Pu, W., Li, G., Huang, X., He, L., Tian, X., Liu, Q., Zhang, L., Wu, S.M., Sucov, H.M.*, et al.* (2016). Endocardium Minimally Contributes to Coronary Endothelium in the Embryonic Ventricular Free Walls. Circ Res *118*, 1880-1893.

Figure 1

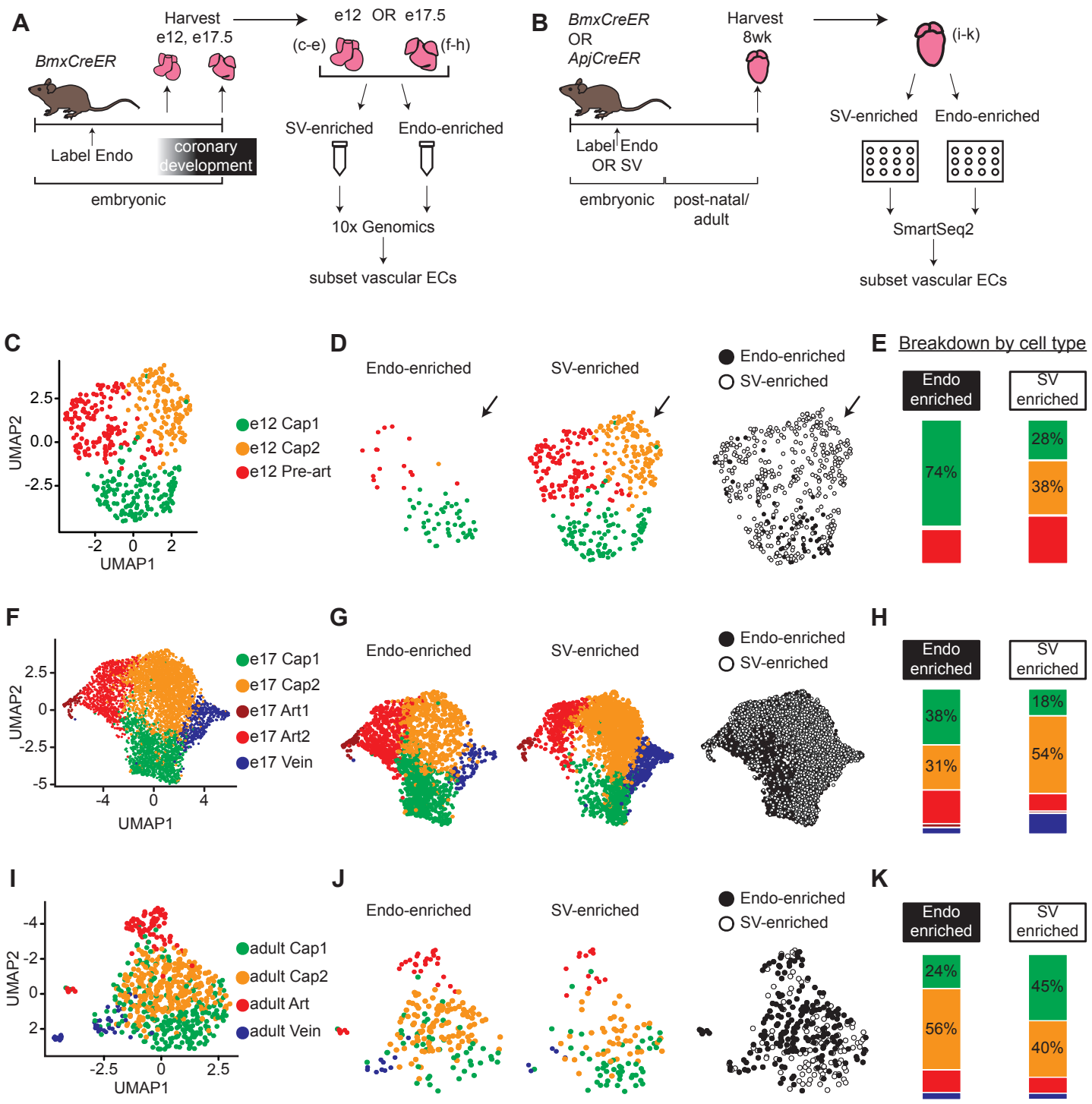
A
Harvest
e12, e17.5
e12 OR e17.5
(c-e)
(f-h)
BmxCreER
Label Endo
coronary development
embryonic
SV-enriched
Endo-enriched
10x Genomics
subset vascular ECs
B
BmxCreER
OR
ApjCreER
Harvest
8wk
(i-k)
Label Endo
OR SV
embryonic
post-natal/
adult
SV-enriched
Endo-enriched
SmartSeq2
subset vascular ECs
C
UMAP2
UMAP1
e12 Cap1
e12 Cap2
e12 Pre-art
D
Endo-enriched
SV-enriched
Endo-enriched
SV-enriched
E
Breakdown by cell type
Endo enriched
SV enriched
74%
28%
38%
F
UMAP2
UMAP1
e17 Cap1
e17 Cap2
e17 Art1
e17 Art2
e17 Vein
G
Endo-enriched
SV-enriched
Endo-enriched
SV-enriched
H
Endo enriched
SV enriched
38%
31%
18%
54%
I
UMAP2
UMAP1
adult Cap1
adult Cap2
adult Art
adult Vein
J
Endo-enriched
SV-enriched
Endo-enriched
SV-enriched
K
Endo enriched
SV enriched
24%
56%
45%
40%

Figure 2

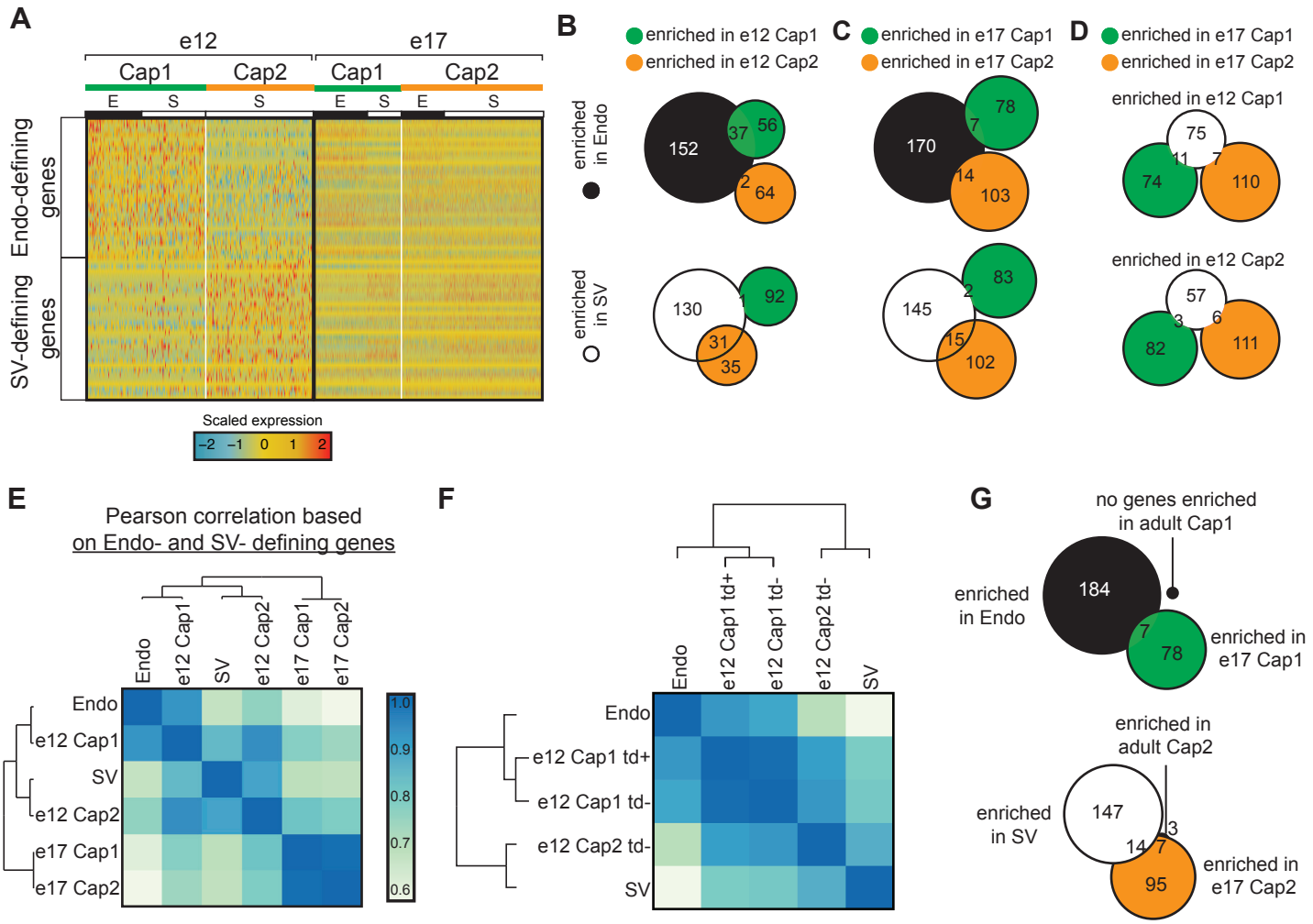
A
e12
e17
Cap1
Cap2
Cap1
Cap2
E
S
S
E
S
E
S
Endo-defining genes
SV-defining genes
Scaled expression
−2 −1 0 1 2
B
enriched in e12 Cap1
enriched in e12 Cap2
enriched in Endo
enriched in SV
152
37
56
2
64
130
1
92
31
35
C
enriched in e17 Cap1
enriched in e17 Cap2
170
7
78
14
103
145
2
83
15
102
D
enriched in e17 Cap1
enriched in e17 Cap2
enriched in e12 Cap1
75
11
7
74
110
enriched in e12 Cap2
57
3
6
82
111
E
Pearson correlation based
on Endo- and SV- defining genes
Endo
e12 Cap1
SV
e12 Cap2
e17 Cap1
e17 Cap2
1.0
0.9
0.8
0.7
0.6
F
Endo
e12 Cap1 td+
e12 Cap1 td-
e12 Cap2 td-
SV
G
no genes enriched
in adult Cap1
enriched
in Endo
184
7
78
enriched in
e17 Cap1
enriched in
adult Cap2
enriched
in SV
147
3
14
7
95
enriched in
e17 Cap2

Figure 3

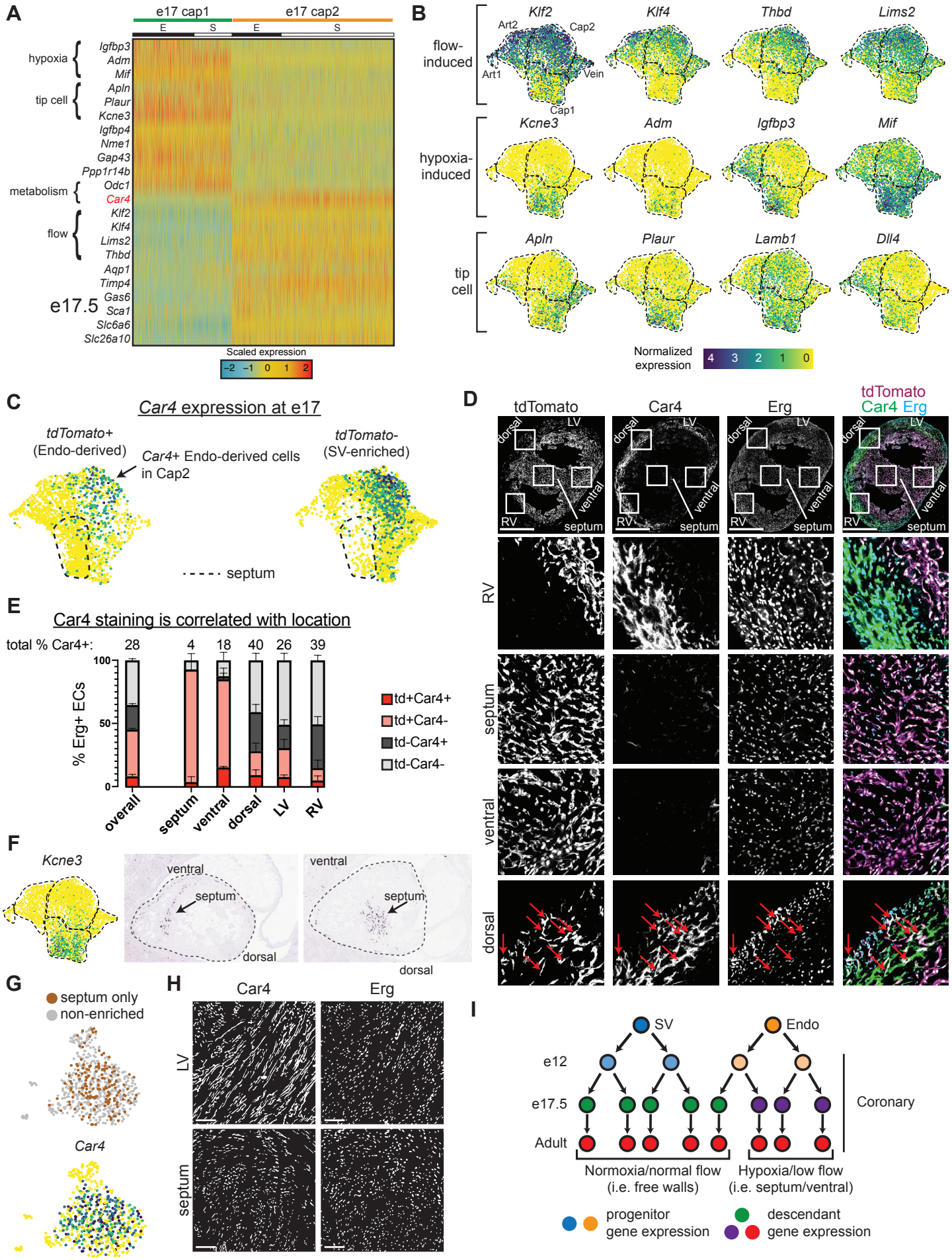
A
e17 cap1
e17 cap2
E
S
E
S
hypoxia
Igfbp3
Adm
Mif
tip cell
Apln
Plaur
Kcne3
Igfbp4
Nme1
Gap43
Ppp1r14b
metabolism
Odc1
Car4
flow
Klf2
Klf4
Lims2
Thbd
Aqp1
Timp4
Gas6
Sca1
Slc6a6
Slc26a10
e17.5
Scaled expression
−2 −1 0 1 2
B
flow-induced
Klf2
Klf4
Thbd
Lims2
Art2
Cap2
Art1
Vein
Cap1
hypoxia-induced
Kcne3
Adm
Igfbp3
Mif
tip cell
Apln
Plaur
Lamb1
Dll4
Normalized expression
4 3 2 1 0
C
Car4 expression at e17
tdTomato+ (Endo-derived)
Car4+ Endo-derived cells in Cap2
tdTomato- (SV-enriched)
septum
D
tdTomato
Car4
Erg
tdTomato Car4 Erg
dorsal
LV
ventral
RV
septum
RV
septum
ventral
dorsal
E
Car4 staining is correlated with location
total % Car4+:
28
4
18
40
26
39
% Erg+ ECs
100
50
0
td+Car4+
td+Car4-
td-Car4+
td-Car4-
overall
septum
ventral
dorsal
LV
RV
F
Kcne3
ventral
septum
dorsal
ventral
septum
dorsal
G
septum only
non-enriched
Car4
H
Car4
Erg
LV
septum
I
SV
Endo
e12
e17.5
Adult
Coronary
Normoxia/normal flow (i.e. free walls)
Hypoxia/low flow (i.e. septum/ventral)
progenitor gene expression
descendant gene expression

Figure 4

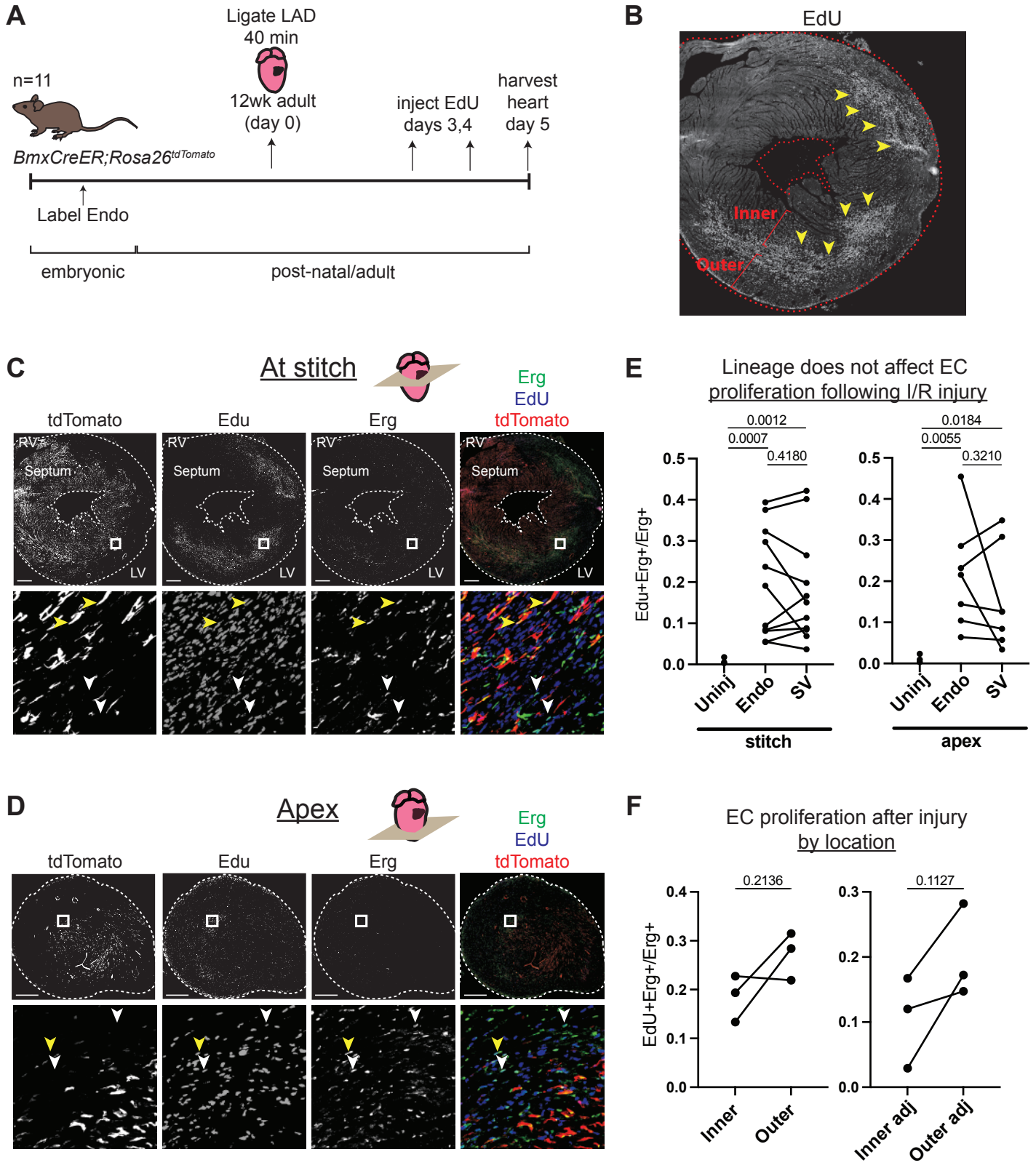
A
Ligate LAD
40 min
n=11
12wk adult
(day 0)
inject EdU
days 3,4
harvest
heart
day 5
BmxCreER;Rosa26tdTomato
Label Endo
embryonic
post-natal/adult
B
EdU
Inner
Outer
C
At stitch
Erg
EdU
tdTomato
tdTomato
Edu
Erg
tdTomato
RV
Septum
LV
D
Apex
Erg
EdU
tdTomato
tdTomato
Edu
Erg
tdTomato
E
Lineage does not affect EC
proliferation following I/R injury
0.0012
0.0007
0.4180
0.0184
0.0055
0.3210
Edu+Erg+/Erg+
Uninj
Endo
SV
stitch
apex
F
EC proliferation after injury
by location
0.2136
0.1127
EdU+Erg+/Erg+
Inner
Outer
Inner adj
Outer adj

Figure 5

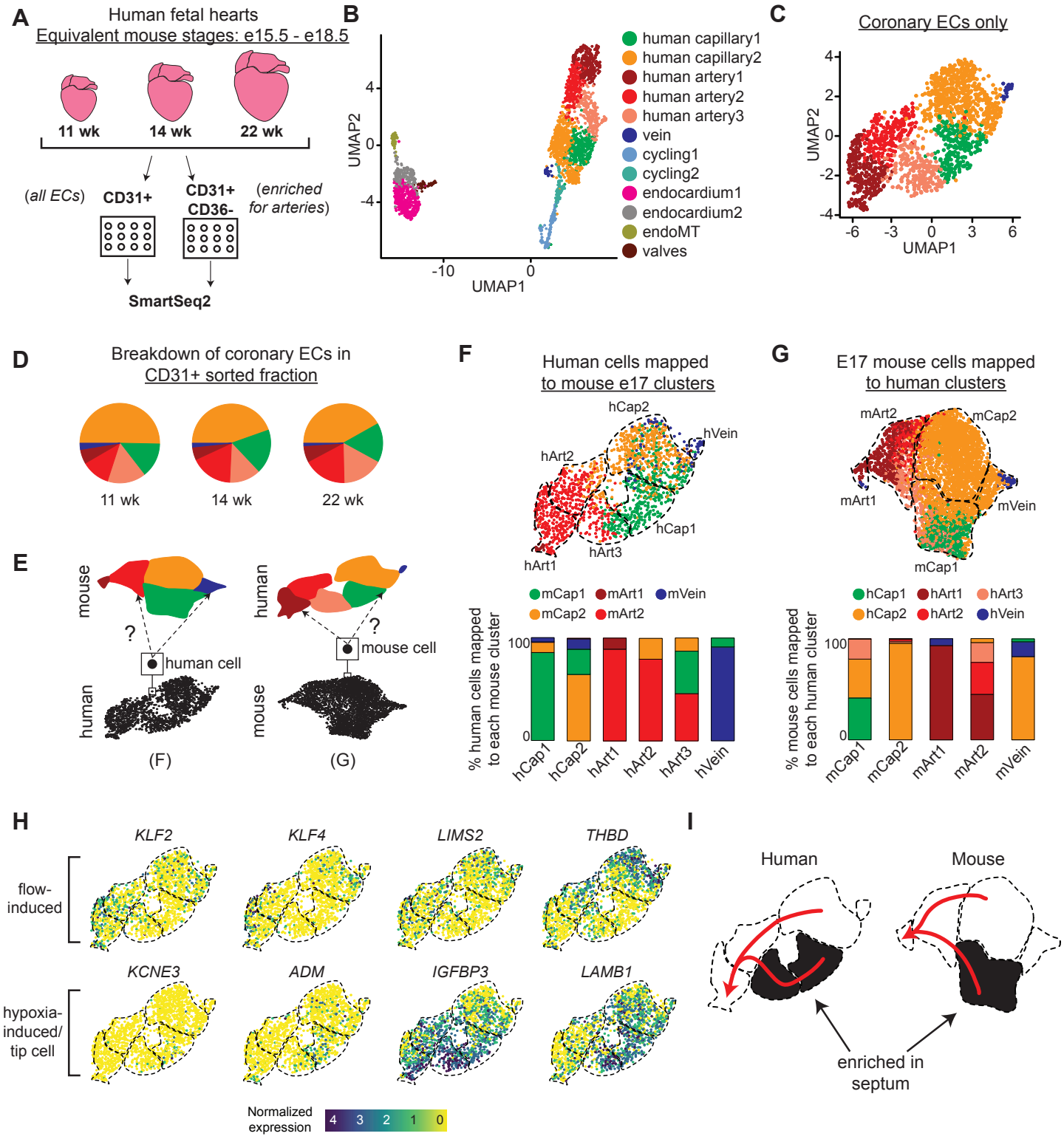
A
Human fetal hearts
Equivalent mouse stages: e15.5 - e18.5
11 wk
14 wk
22 wk
(all ECs)
CD31+
CD31+
CD36-
(enriched for arteries)
SmartSeq2
B
UMAP2
UMAP1
human capillary1
human capillary2
human artery1
human artery2
human artery3
vein
cycling1
cycling2
endocardium1
endocardium2
endoMT
valves
C
Coronary ECs only
UMAP2
UMAP1
D
Breakdown of coronary ECs in
CD31+ sorted fraction
11 wk
14 wk
22 wk
E
mouse
human
human cell
human
mouse
mouse cell
(F)
(G)
F
Human cells mapped
to mouse e17 clusters
hCap2
hVein
hArt2
hCap1
hArt3
hArt1
mCap1
mArt1
mVein
mCap2
mArt2
% human cells mapped
to each mouse cluster
hCap1
hCap2
hArt1
hArt2
hArt3
hVein
G
E17 mouse cells mapped
to human clusters
mArt2
mCap2
mArt1
mVein
mCap1
hCap1
hArt1
hArt3
hCap2
hArt2
hVein
% mouse cells mapped
to each human cluster
mCap1
mCap2
mArt1
mArt2
mVein
H
KLF2
KLF4
LIMS2
THBD
flow-induced
KCNE3
ADM
IGFBP3
LAMB1
hypoxia-induced/ tip cell
Normalized expression
4 3 2 1 0
I
Human
Mouse
enriched in septum

Figure 6

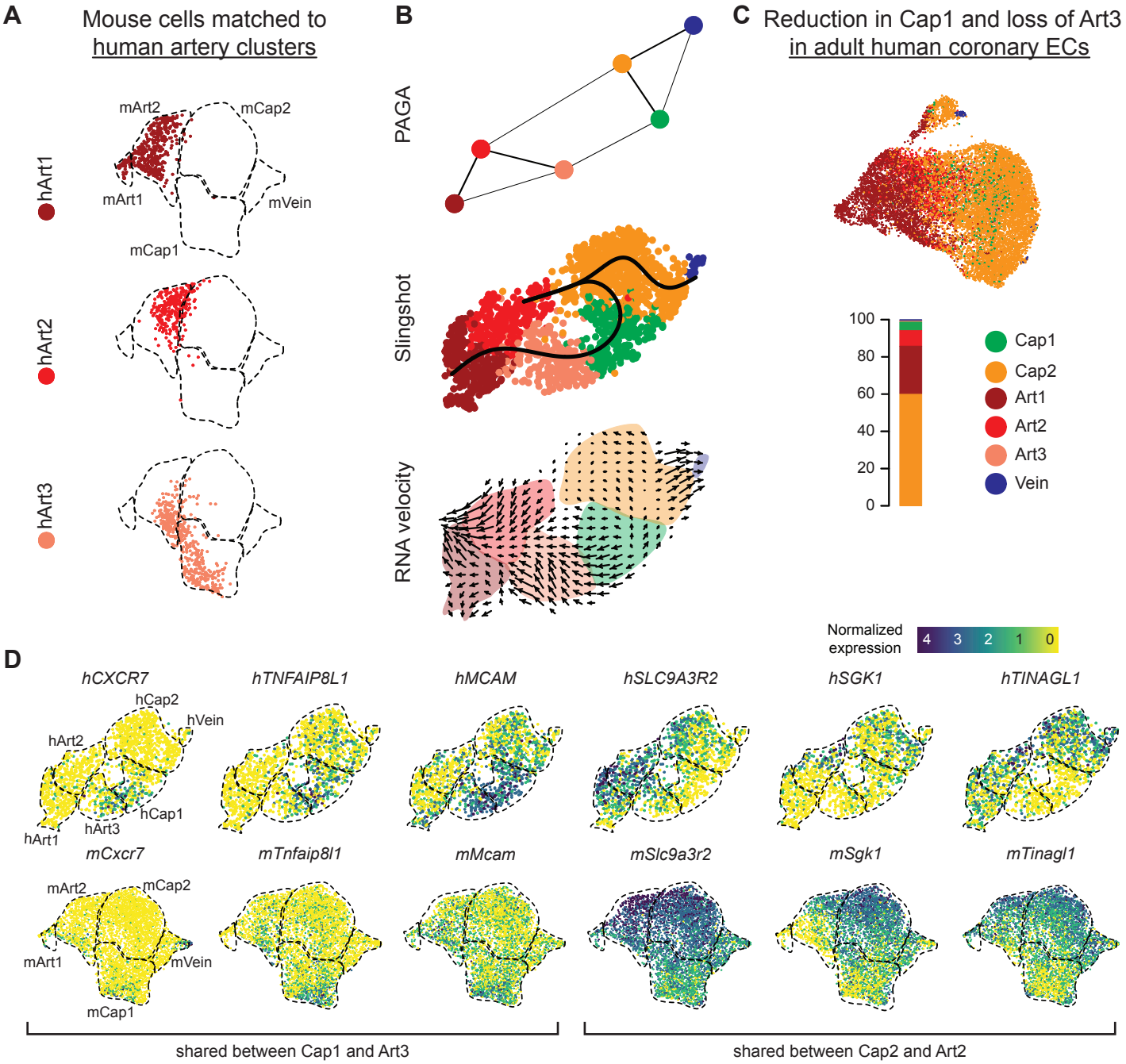
A
Mouse cells matched to
human artery clusters
mArt2
mCap2
mArt1
mVein
mCap1
hArt1
hArt2
hArt3
B
PAGA
Slingshot
RNA velocity
C
Reduction in Cap1 and loss of Art3
in adult human coronary ECs
100
80
60
40
20
0
Cap1
Cap2
Art1
Art2
Art3
Vein
D
Normalized
expression
4 3 2 1 0
hCXCR7
hTNFAIP8L1
hMCAM
hSLC9A3R2
hSGK1
hTINAGL1
hCap2
hVein
hArt2
hCap1
hArt3
hArt1
mCxcr7
mTnfaip8l1
mMcam
mSlc9a3r2
mSgk1
mTinagl1
mArt2
mCap2
mArt1
mVein
mCap1
shared between Cap1 and Art3
shared between Cap2 and Art2

Figure 7

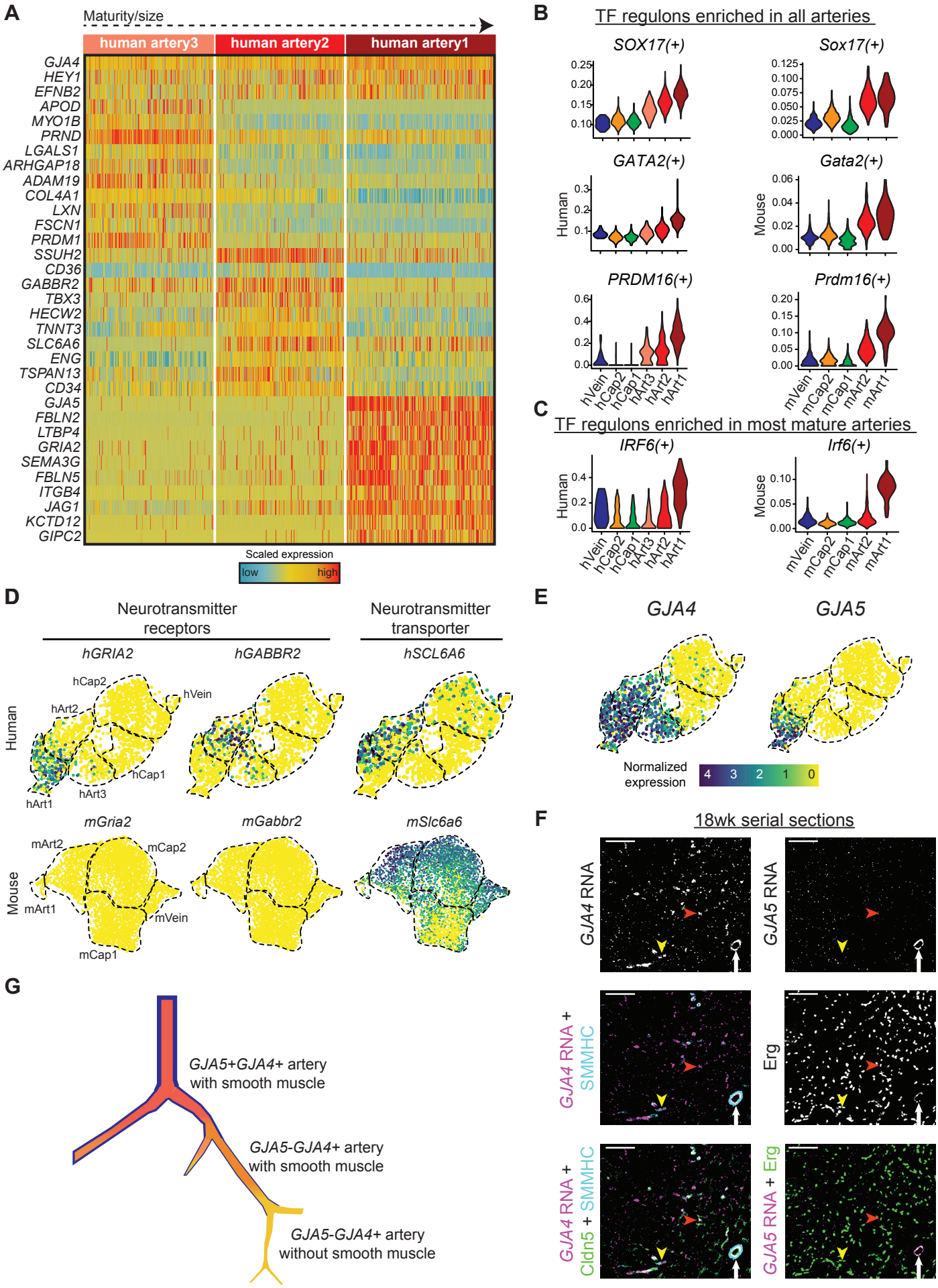
A
Maturity/size
human artery3
human artery2
human artery1
GJA4
HEY1
EFNB2
APOD
MYO1B
PRND
LGALS1
ARHGAP18
ADAM19
COL4A1
LXN
FSCN1
PRDM1
SSUH2
CD36
GABBR2
TBX3
HECW2
TNNT3
SLC6A6
ENG
TSPAN13
CD34
GJA5
FBLN2
LTBP4
GRIA2
SEMA3G
FBLN5
ITGB4
JAG1
KCTD12
GIPC2
Scaled expression
low
high
B
TF regulons enriched in all arteries
SOX17(+)
Sox17(+)
GATA2(+)
Gata2(+)
PRDM16(+)
Prdm16(+)
Human
Mouse
hVein
hCap2
hCap1
hArt3
hArt2
hArt1
mVein
mCap2
mCap1
mArt2
mArt1
C
TF regulons enriched in most mature arteries
IRF6(+)
Irf6(+)
D
Neurotransmitter receptors
Neurotransmitter transporter
hGRIA2
hGABBR2
hSCL6A6
mGria2
mGabbr2
mSlc6a6
E
GJA4
GJA5
Normalized expression
4
3
2
1
0
F
18wk serial sections
GJA4 RNA
GJA5 RNA
GJA4 RNA + SMMHC
Erg
GJA4 RNA + Cldn5 + SMMHC
GJA5 RNA + Erg
G
GJA5+GJA4+ artery with smooth muscle
GJA5-GJA4+ artery with smooth muscle
GJA5-GJA4+ artery without smooth muscle

Table 1. Genes unique to human coronary ECs

SLC14A1
GABBR2
NRN1
EPHA3
ADMTSL1
A2M
PRND
GRIA2
KCNN3
SERPINE2
LPCAT2
LGALS3
APOA1
SYNJ2
OCIAD2
PRICKLE2
CTNND1
IFITM2

Supplementary figure 1

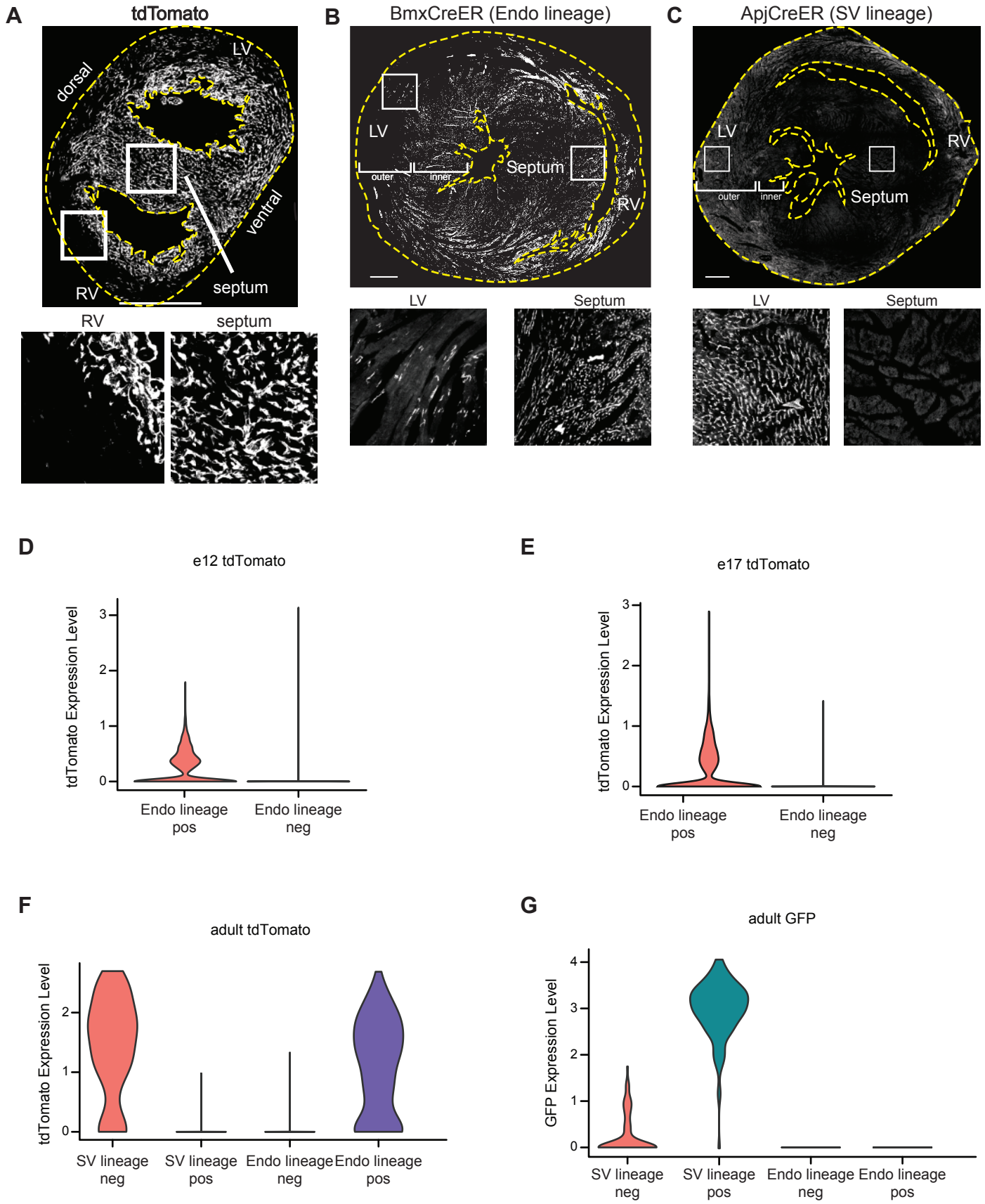

Supplementary figure 2

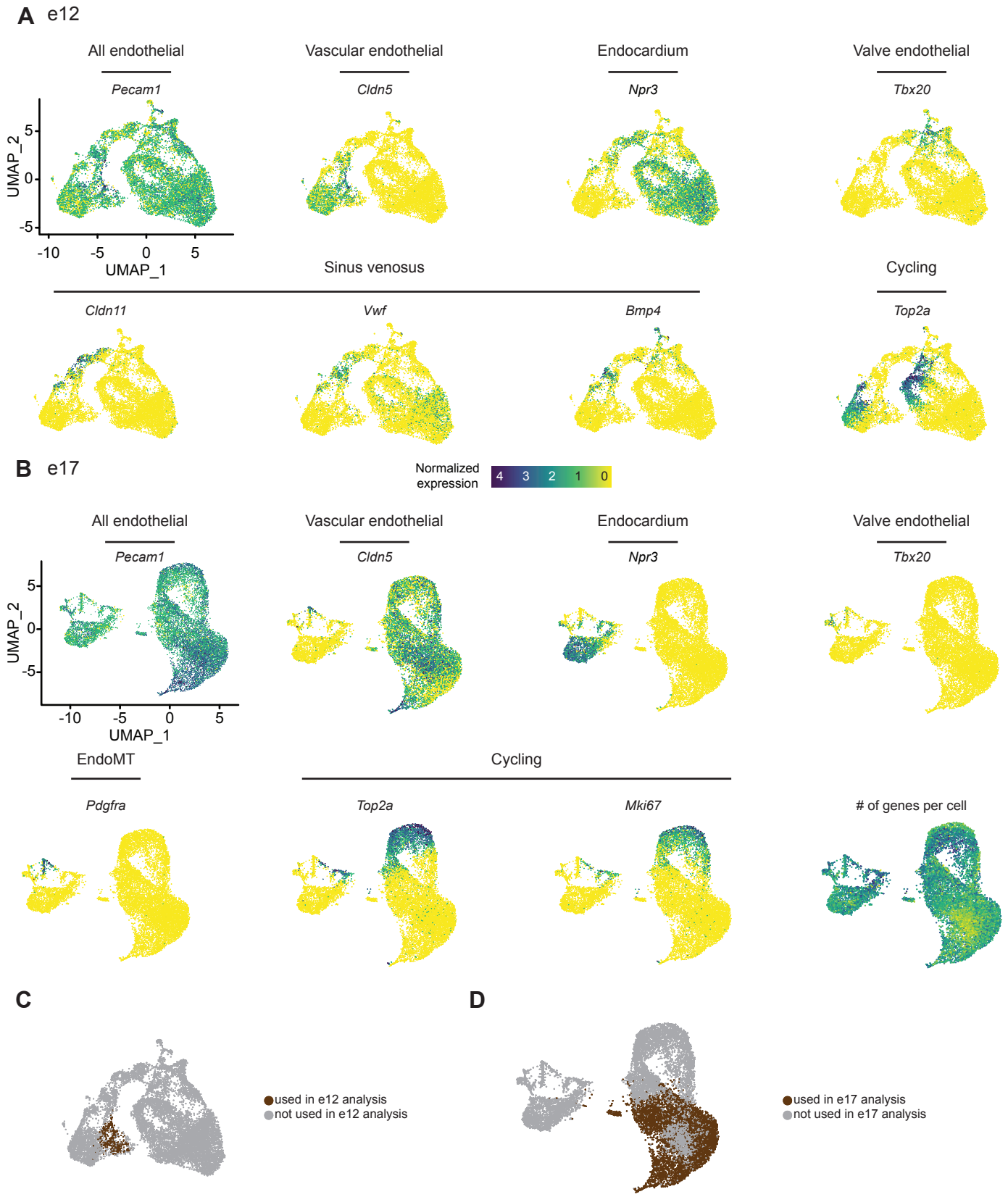

Supplementary figure 3

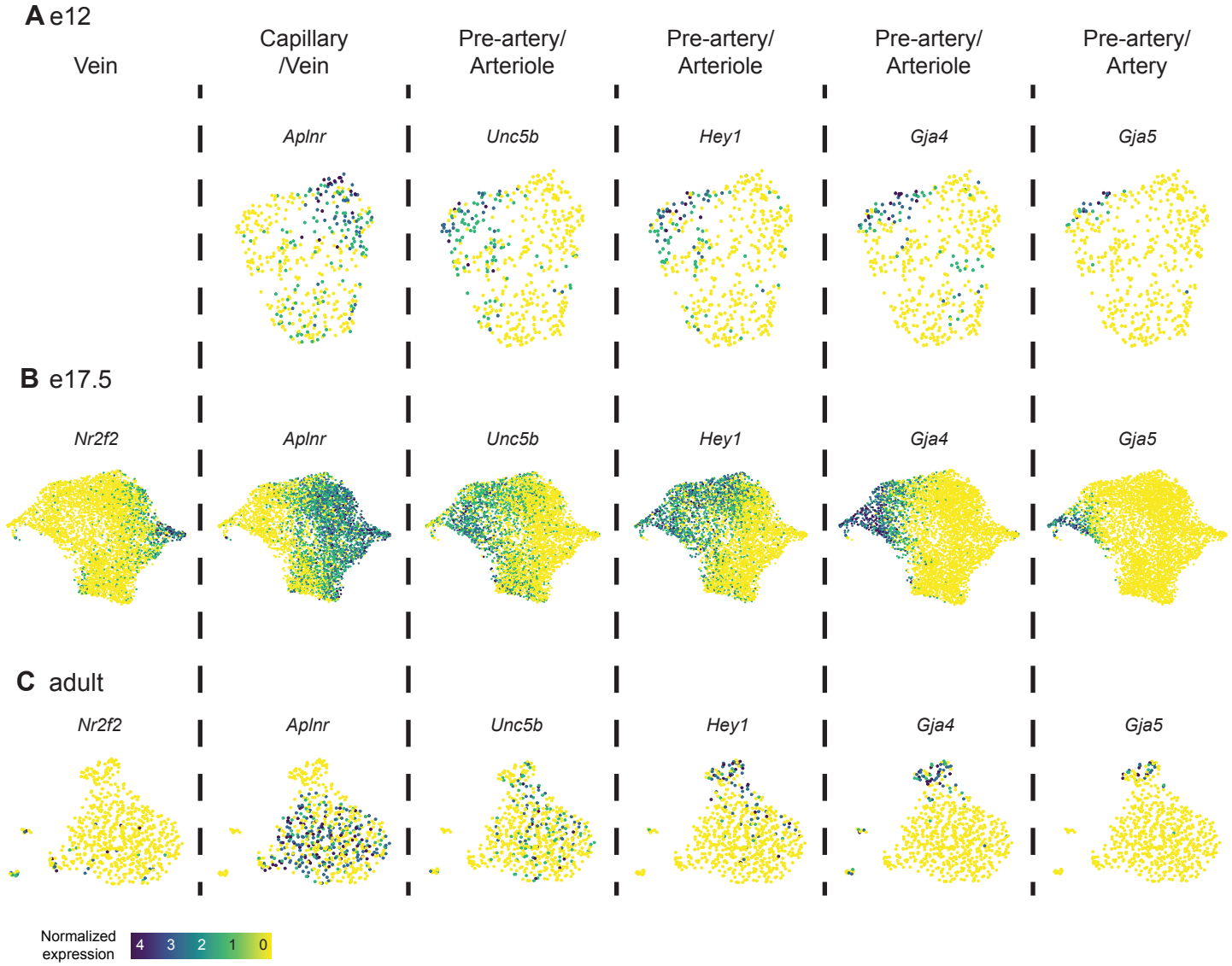

Supplementary figure 4

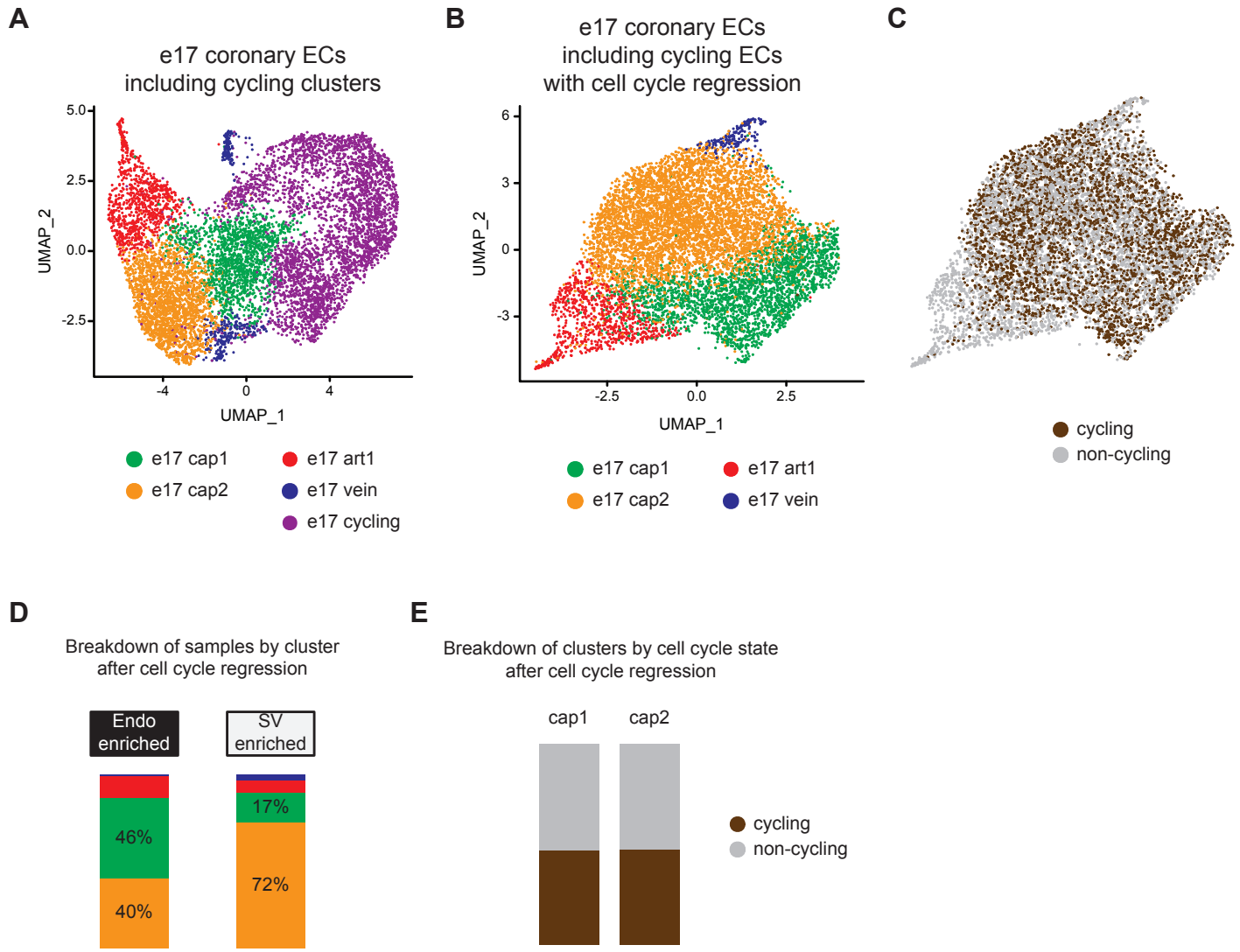

Supplementary figure 5

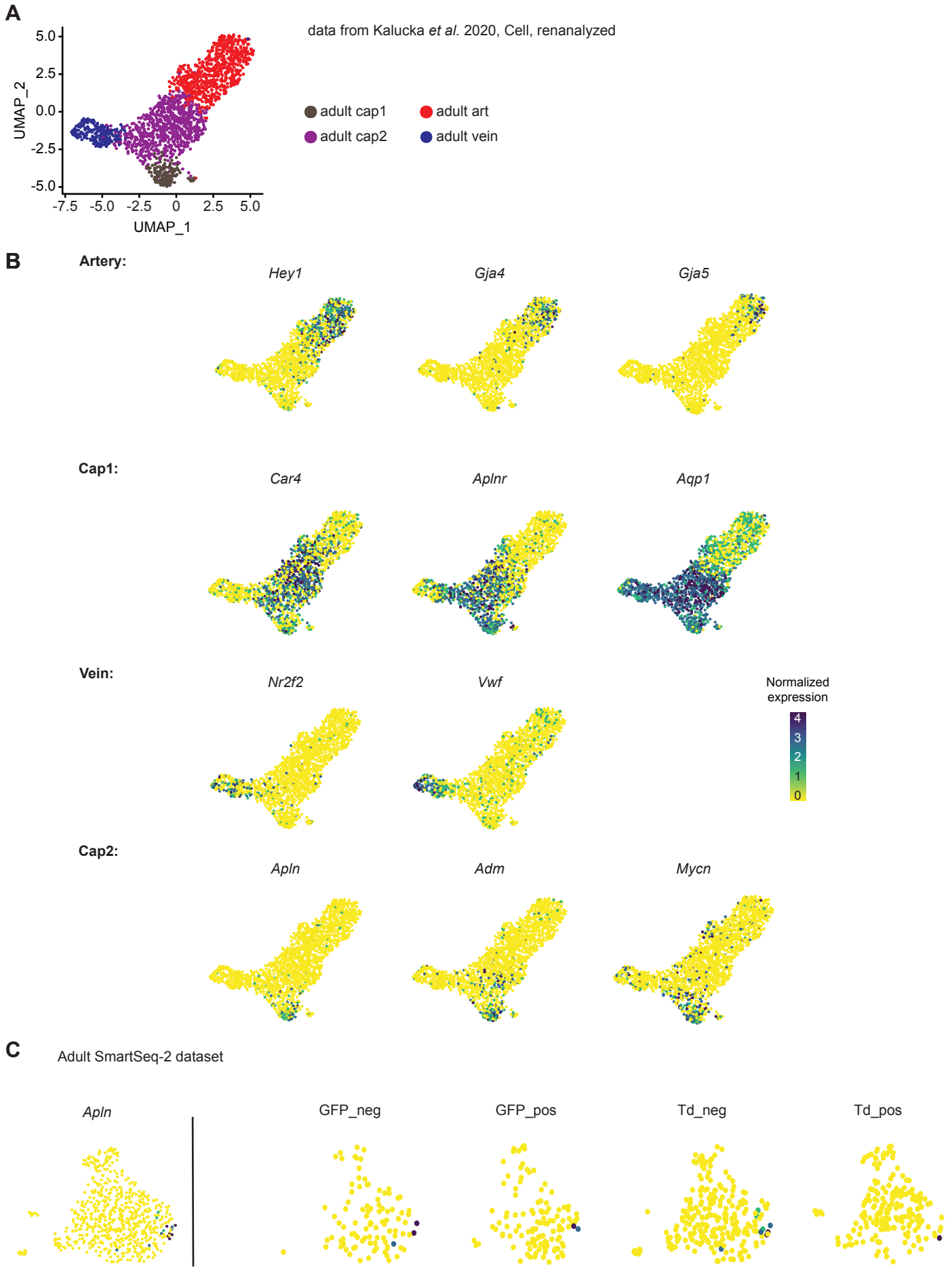

Supplementary figure 6

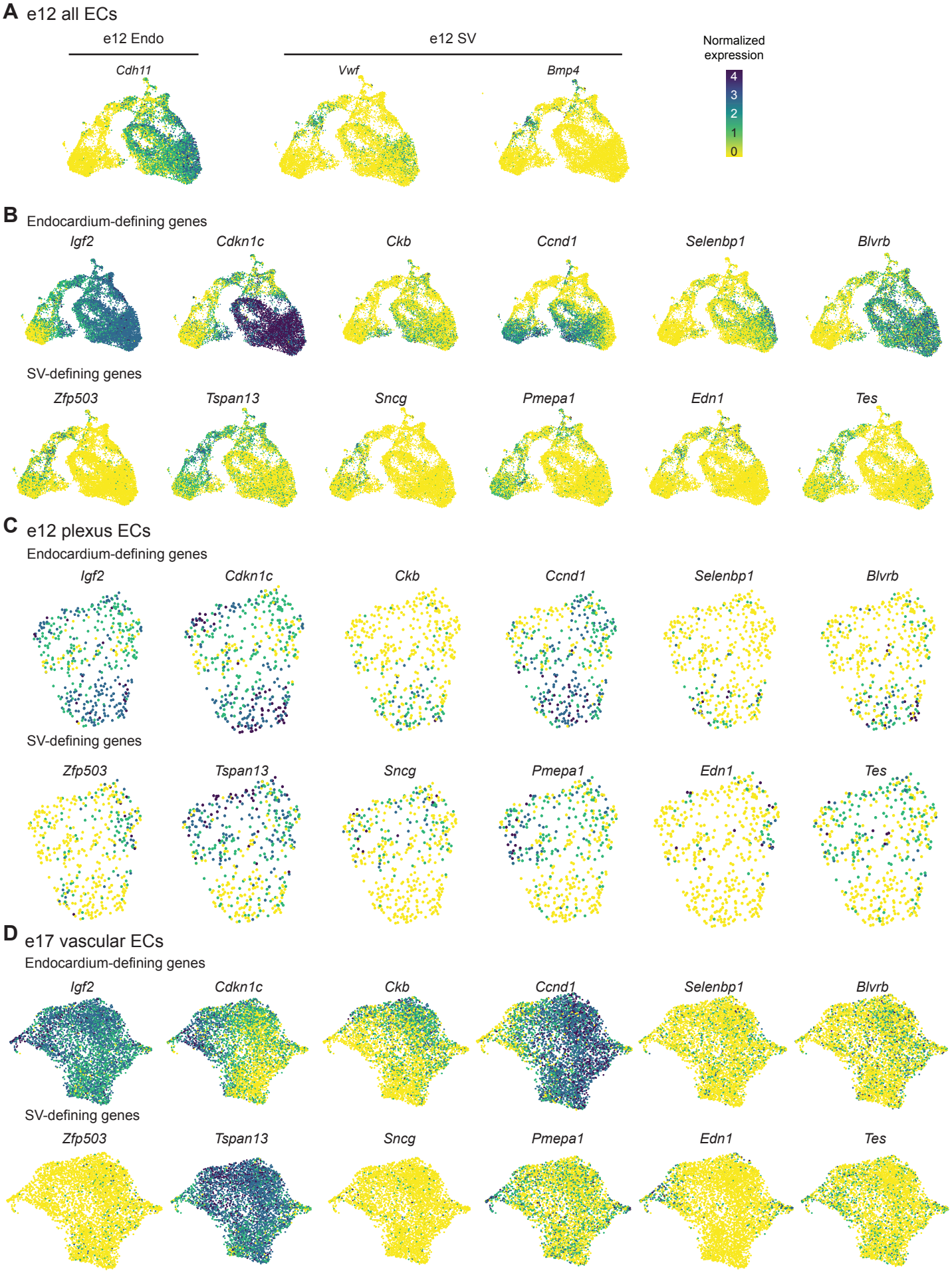

Supplementary figure 7

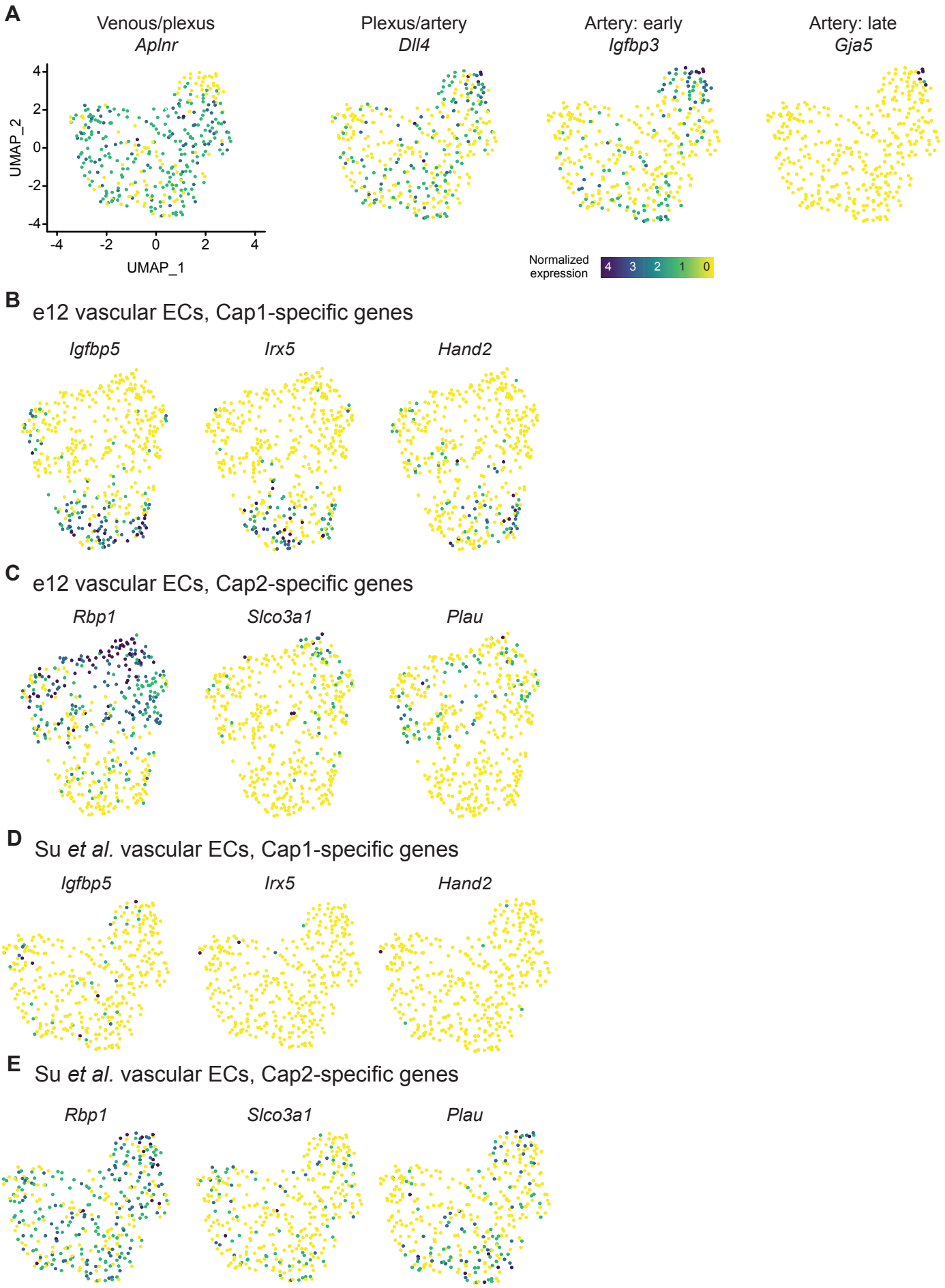

Supplementary figure 8

A Expression of flow-induced genes at e17

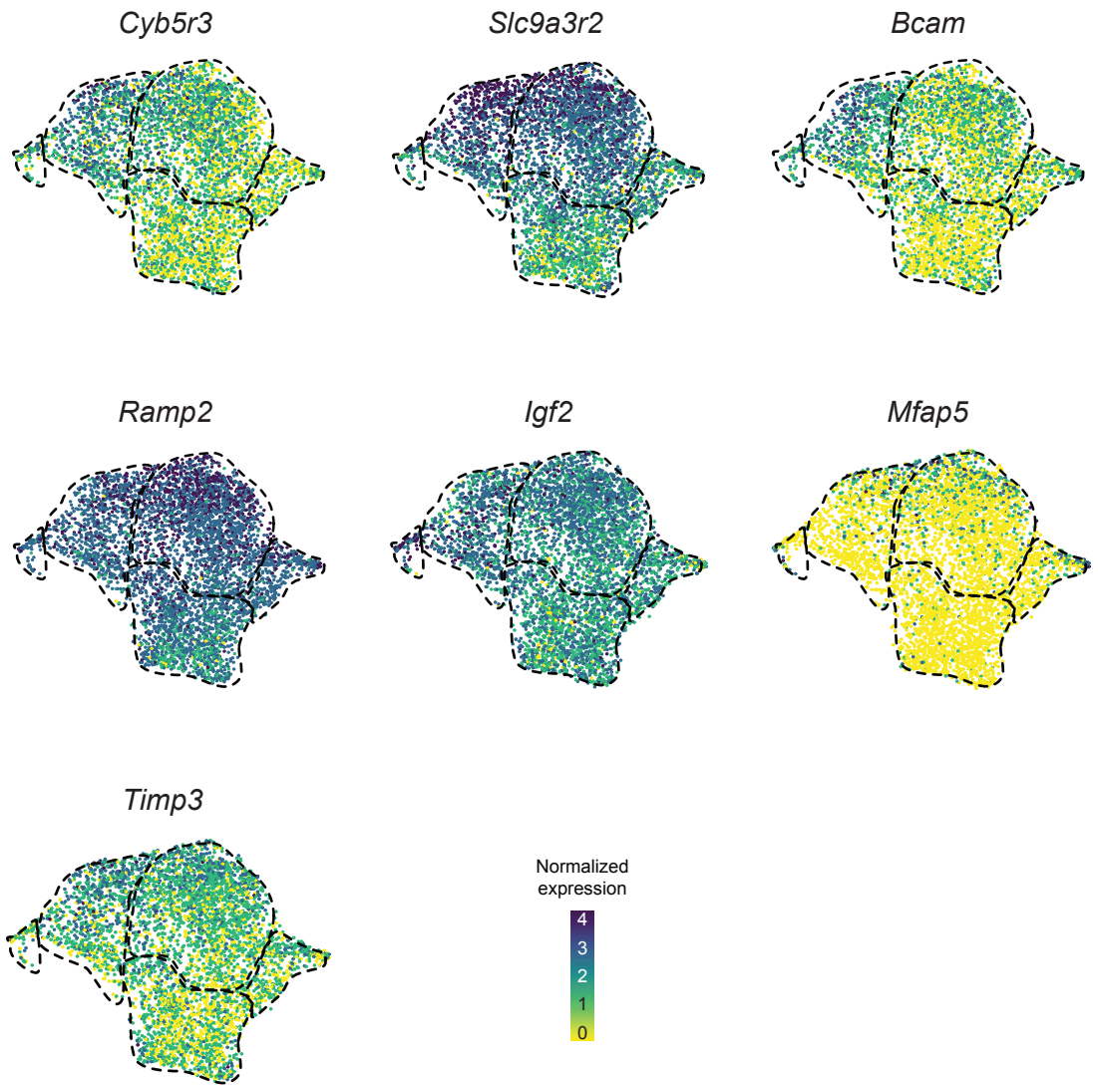

Supplementary figure 9

A Endocardium-enriched genes that are higher in septum:

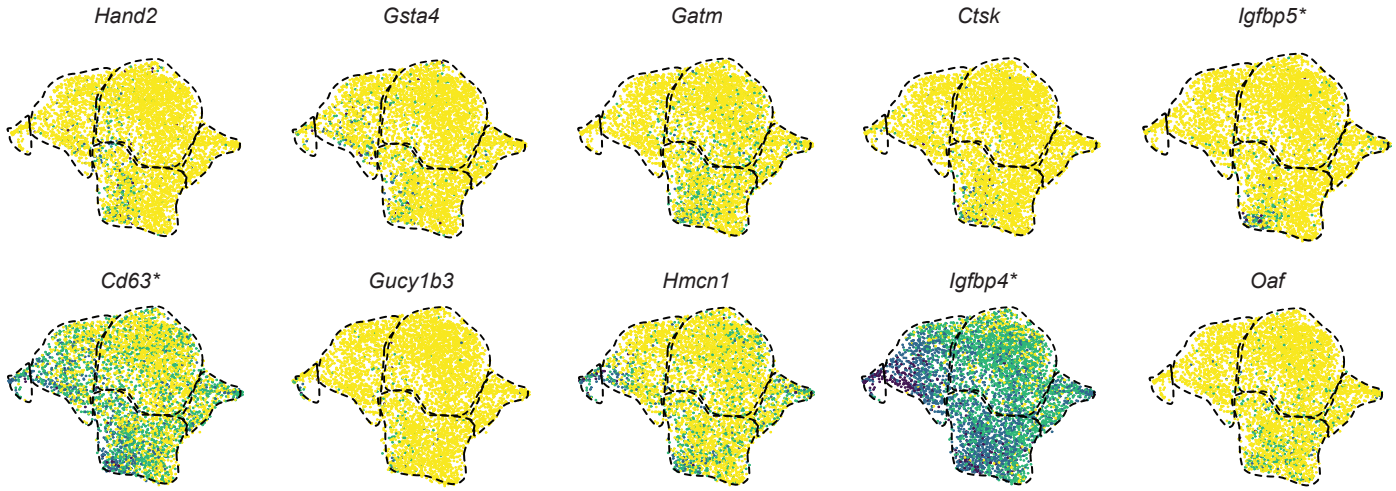

B SV-enriched genes that are lower in septum:

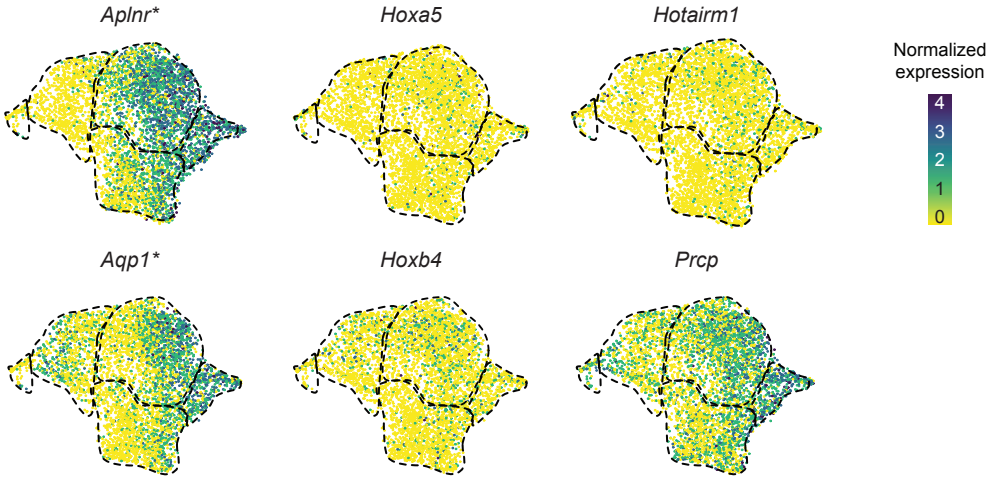

C SV-enriched genes that are higher in Cap2:

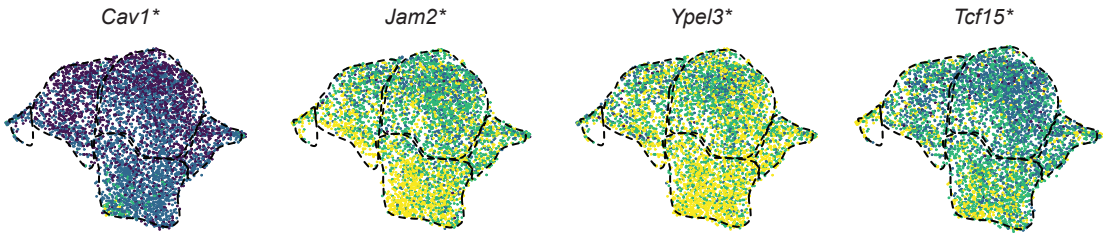

Supplementary figure 10

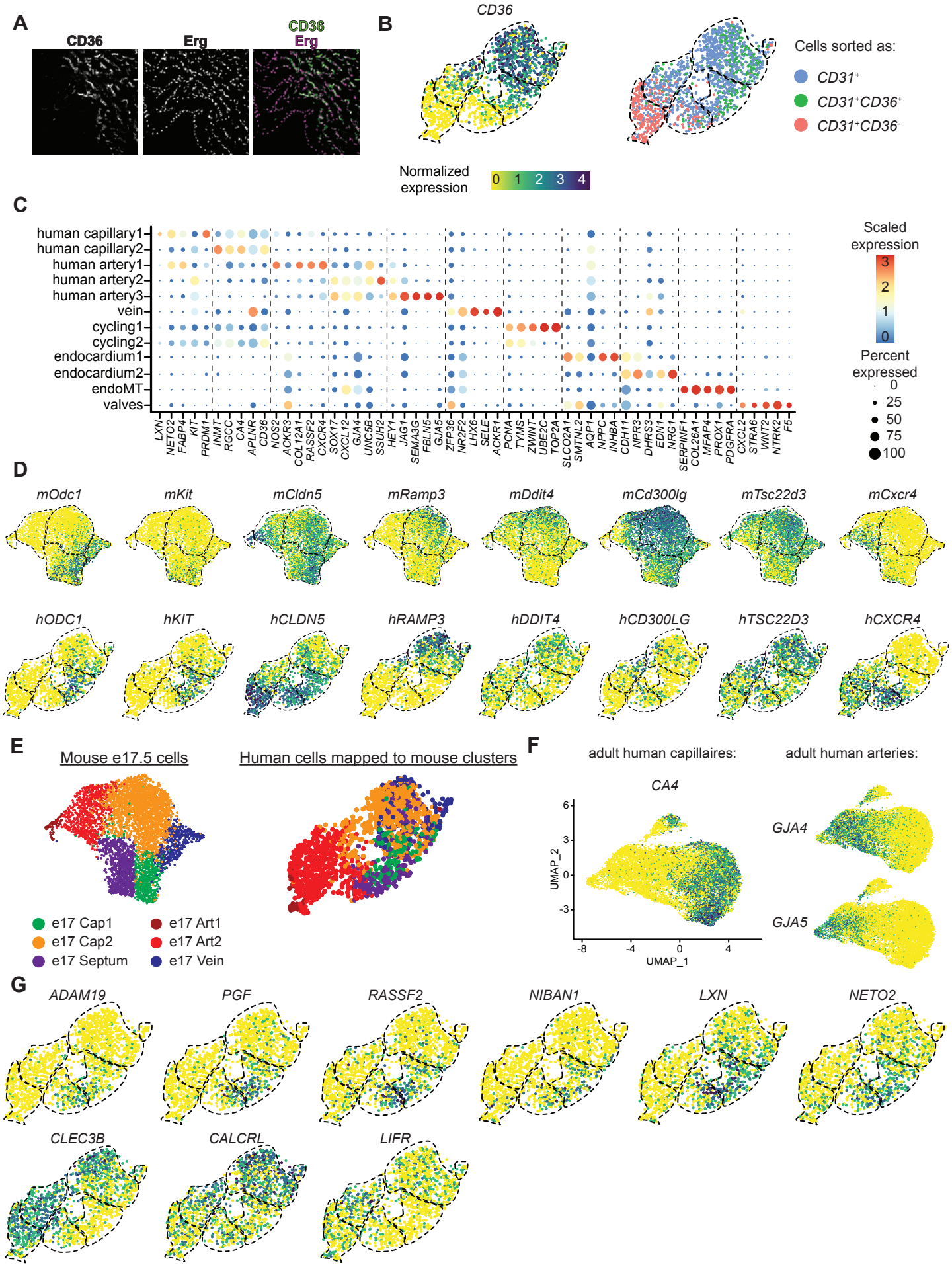
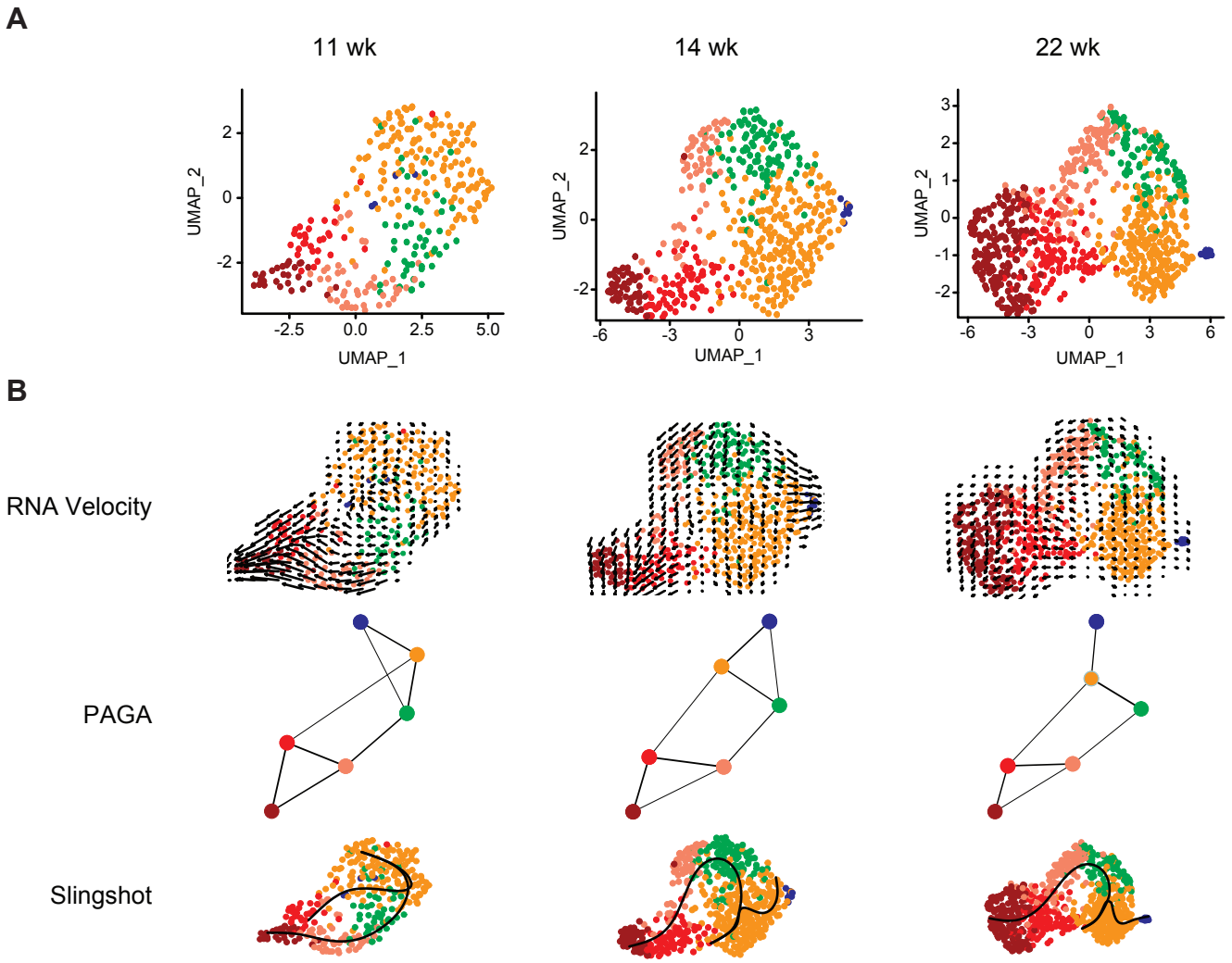
Supplementary figure 11